Multifidelity Computer Model Emulation with High-Dimensional Output: An Application to Storm Surge

Pulong Ma*^{1,2}, Georgios Karagiannis³, Bledar A. Konomi⁴, Taylor G. Asher⁵, Gabriel R. Toro⁶, and Andrew T. Cox⁷

¹The Statistical and Applied Mathematical Sciences Institute

²Duke University

³Durham University

⁴University of Cincinnati

⁵University of North Carolina at Chapel Hill

⁶Lettis Consultants International, Inc.

⁷Oceanweather, Inc.

Abstract

Hurricane-driven storm surge is one of the most deadly and costly natural disasters, making precise quantification of the surge hazard of great importance. Inference of such systems is done through physics-based computer models of the process. Such surge simulators can be implemented with a wide range of fidelity levels, with computational burdens varying by several orders of magnitude due to the nature of the system. The danger posed by surge makes greater fidelity highly desirable, however such models and their high-volume output tend to come at great computational cost, which can make detailed study of coastal flood hazards prohibitive. These needs make the development of an emulator combining high-dimensional output from multiple complex computer models with different fidelity levels important. We propose a parallel partial autoregressive cokriging model to predict highly-accurate storm surges in a computationally efficient way over a large spatial domain. This emulator has the capability of predicting storm surges as accurately as a high-fidelity computer model given any storm characteristics and allows accurate assessment of the hazards from storm surges over a large spatial domain. R codes are provided to show the numerical results through an R package called ARCokrig.

^{*}Correspondence to: Pulong Ma, Postdoctoral Fellow at the Statistical and Applied Mathematical Sciences Institute and Duke University; 79 T.W. Alexander Drive, 4501 Research Commons, Suite 300, P.O. Box 110207, Research Triangle Park, NC 27709; Email: pulong.ma@duke.edu

Keywords: Autoregressive cokriging; High-dimensional output; Multifidelity computer model; Storm surge; Uncertainty quantification

1 Introduction

Storm surge is one of the most severe natural disasters that can lead to significant flooding in coastal areas that brings multi-billion dollar damages and is responsible on average for half of lives lost from hurricanes (Rappaport, 2014). On average, inflation-normalized direct economic damages to the U.S. (1900-2005) are estimated at \$10 billion per year and increasing as a result of storm surges (Pielke Jr et al., 2008; Klotzbach et al., 2018). Since 2005, there have been 12 hurricanes whose total U.S. damages exceeded \$10 billion (NOAA National Centers for Environmental Information, 2019). For instance, Hurricane Katrina (2005) caused over 1500 deaths and total estimated damages of \$75 billion in the New Orleans area and along the Mississippi coast as a result of storm surge (FEMA, 2006). To mitigate these impacts, studies are carried out to evaluate the probabilistic hazard (e.g. Niedoroda et al., 2010; Cialone et al., 2017; Garner et al., 2017) and risk (e.g. Aerts et al., 2013; Fischbach et al., 2016) from coastal flooding through a synthesis of computer modeling, statistical modeling, and extreme-event probability computation. These studies support development and application of flood insurance rates, building codes, land use planning/development, infrastructure design and construction, and related goals. Similarly, forecast simulations are used to support a wide array of operational needs, most notably disaster mitigation and evacuation planning/preparedness (e.g. Blanton et al., 2018; Georgas et al., 2016).

The ADCIRC ocean circulation model (Luettich and Westerink, 2004; Westerink et al., 2008) is the primary model in the U.S. to predict storm surges in coastal areas. It was certified by the Federal Emergency Management Agency (FEMA) for coastal flood hazard study and has been successfully used in a large number of applications, including FEMA flood hazard map updates (e.g., FEMA, 2008; Niedoroda et al., 2010; Jensen et al., 2012;

Hesser et al., 2013) and in support of United States Army Corps of Engineers (USACE) projects (e.g., Bunya et al., 2010; Wamsley et al., 2013; Cialone et al., 2017).

In storm surge risk assessments, ADCIRC needs to be run for a large number of storm characteristics. ADCIRC can be run at different levels of accuracy due to the sophistication of the physics incorporated in mathematical models, accuracy of numerical solvers, and resolutions of meshes. Although ADCIRC can be run efficiently in parallel on large supercomputers (Tanaka et al., 2011), its computational cost scales with the cube of the spatial resolution, meaning that very high fidelity models are several orders of magnitude more expensive than lower fidelity ones. By incorporating the physics of ocean waves, ADCIRC can generate storm surges with even greater fidelity, but this adds another order of magnitude to the run time as compared to the uncoupled ADCIRC model (Dietrich et al., 2012). For instance, a single high-resolution, coupled simulation in Southwestern Florida takes roughly 2000 core-hours on a high-performance supercomputer (Towns et al., 2014). As a result, research often uses coarser models without wave effects, even though the importance of more advanced, detailed models in estimating storm surge has been well-demonstrated (e.g. Dietrich et al., 2010; Marsooli and Lin, 2018; Yin et al., 2016).

An important scientific demand is to develop an *emulator* - a fast probabilistic approximation of a simulator - that can produce highly accurate storm surges over a large spatial domain. The need to support such improvements is particularly great in probabilistic flood studies dealing with climate change where a broad host of variables need to be considered. For instance, risk studies with relatively simple surge models estimate the current coastal flooding risk to New York City alone at over 100 million U.S. dollars per year (Aerts et al., 2013, 2014). But these estimates are highly sensitive to underlying assumptions that remain to be explored (e.g. de Moel and Aerts, 2011; Fischbach et al., 2016). Hurricane Sandy's damages to New York City were 30% higher than they otherwise would have been due to the 20 cm of sea level rise that have occurred over the past century (Lloyds of London report). Similarly, high-fidelity studies of coastal flooding changes associated with sea level

rise and/or climate change have shown complex, nonlinear changes in flooding patterns that simpler studies cannot uncover (Liu et al., 2019; Garner et al., 2017; Bilskie et al., 2019).

The main scientific goal in this article is to develop an emulator that can not only predict highly accurate storm surges over a large spatial domain but also can be run very quickly to support coastal flood hazard studies. The development of an emulator for the high-fidelity storm surge model directly can be computationally prohibitive, since the high-fidelity storm surge model requires a tremendous amount of computing resources just to obtain a single run. An alternative is to develop an emulator that can combine a limited number of highly accurate simulations from a high-fidelity but expensive surge model and a larger number of less accurate simulations from a low-fidelity but cheaper surge model. Combining simulations from different fidelity levels relies on the idea that, after quantifying discrepancy between models of different fidelity levels, information from the low-fidelity surge model can facilitate prediction at high fidelity.

Several statistical works have been proposed to combine output from simulators at different fidelity levels based on a well-known geostatistical method called *cokriging* (see Chapter 3 of Cressie, 1993). The idea to emulate multiple computer models is originated in Kennedy and O'Hagan (2000) using an autoregressive cokriging model. The work in Kennedy and O'Hagan (2000) has been extended in several ways. For instance, Qian and Wu (2008) propose a Bayesian hierarchical formulation. Le Gratiet (2013) devises an efficient Bayesian approach to estimate model parameters. Konomi and Karagiannis (2019) introduce nonstationarity by partitioning the input space via a Bayesian tree structure. Ma (2019) develops objective Bayesian analysis for an autoregressive cokriging model. All these works focus on univariate computer model output.

Building upon a univariate autoregressive cokriging model, we propose a multivariate autoregressive cokriging model that can deal with high-dimensional output under non-nested design. We also develop an empirical Bayesian approach to facilitating inference via a

data-augmentation technique. To estimate model parameters, we devise a Monte Carlo expectation-maximization (MCEM) algorithm. To make prediction, we devise a sequential prediction approach in which prediction at a higher fidelity level requires prediction to be made at a lower fidelity level. This multivariate formulation explicitly introduces nonstationarity to model the mean parameters and variance parameters in Gaussian processes at each fidelity level. Inference in the multivariate autoregressive cokriging model is computationally efficient as demonstrated in the storm surge application.

The proposed methodology can also be implemented to address a wide range of applications in physics and engineering where interest lies in predicting real-world processes while taking into account high-dimensional computer model output at different levels of fidelity. This article develops a computationally efficient approach for synthesizing highly multivariate output from multiple computer models. Statistical inference based on the proposed model is accomplished in an empirical Bayesian framework.

The remainder of the article is organized as follows. Section 2 introduces the storm surge application with two storm surge simulators. In Section 3, we present the proposed methodology to handle high-dimensional output and non-nested design. In Section 4, an analysis of storm surge simulators is performed with the proposed methodology. Section 5 is concluded with discussions and possible extensions.

2 Motivating Application: Storm Surge

2.1 Storm Surge Simulators

ADCIRC is a hydrodynamic circulation numerical model that solves the shallow-water equations for water levels and horizontal currents using the finite-element method over an unstructured gridded domain representing bathymetric and topographic features (Luettich and Westerink, 2004). Information about ADCIRC can be accessed at https://adcirc.org.

In what follows, we will refer to ADCIRC as the low-fidelity simulator, meanwhile we will refer to the coupled SWAN + ADCIRC model as the high-fidelity simulator. The latter incorporates the Simulating WAves Nearshore (SWAN) wave model (Booij et al., 1999; Zijlema, 2010) in order to enhance system physics and accuracy. This is achieved by tightly coupling the ADCIRC and SWAN models, simulating them on the same unstructured mesh (Dietrich et al., 2011, 2012). This coupling is important to accurate prediction of waves in the nearshore, which ride on top of storm surge and bring substantial destructive power to coastal structures and defenses. The coupling also enhances storm surge because, as storm waves break in shallow water, there is also a change in radiation stress gradients, which tends to further enhance the shoreward momentum flux (Longuet-Higgins and Stewart, 1964). The coupled SWAN + ADCIRC model has been validated to observed surges in several studies for historical storms, and shows good model performance with typical errors below 0.3 meters (Dietrich et al., 2012, 2011, 2010; FEMA, 2017; Cialone et al., 2017).

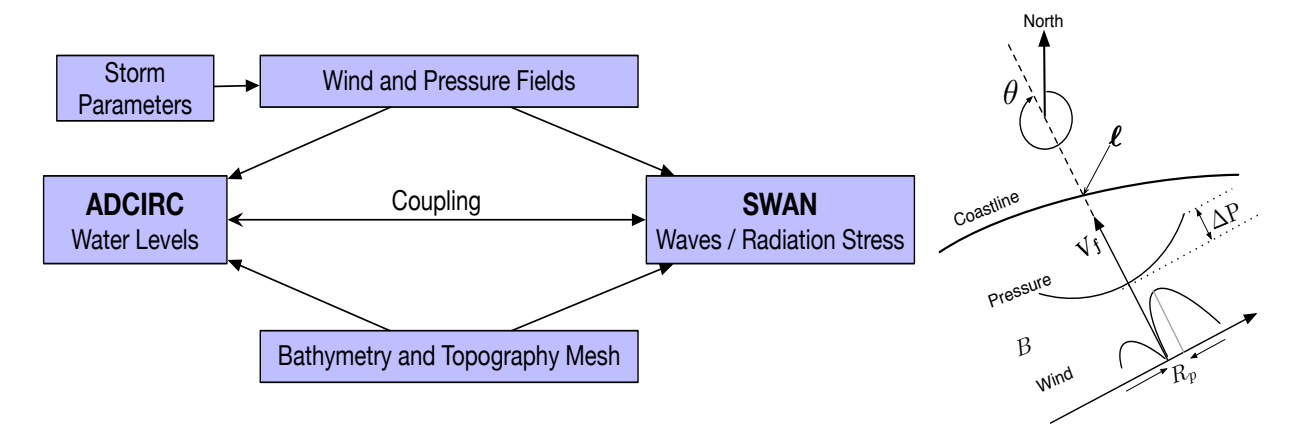


Fig. 1. Diagram of storm surge models based on ADCIRC and storm parameters. The left panel shows ADCIRC and its coupling with SWAN. Then right panel shows storm parameters when a storm approaches the coastline (Toro et al., 2010). ADCIRC has bathymetry and topography mesh and wind and pressure fields as inputs. Storm parameters are used to derive the wind and pressure fields.

Figure 1 shows a basic diagram for the ADCIRC simulator and the SWAN + ADCIRC simulator. In this study, we focus on six input parameters to characterize the storm: ΔP ,

 R_p , V_f , θ , B, ℓ , with their physical meaning given in Table 1. These parameters will be treated as inputs in the ADCIRC simulator. Although the behavior of hurricanes is much more complex than this characterization, using this simplified storm parameterization is acceptable for the probabilistic characterization of future storms since no practical or robust model exists to represent these effects for surge-frequency calculations for future storms. In this application, the response variable of interest is the peak surge elevation (PSE) for the landfalling hurricane simulated from these surge models, where the peakness is taken across time over the course of one storm.

Table 1. Storm characteristics parameters.

Input variables	Physical meaning
ΔP	central pressure deficit of the storm (mb)
R_p	scale pressure radius in nautical miles
V_f	storm's forward speed (m/s)
heta	storm's heading in degrees clockwise from north
B	Holland's B parameter (unitless)
ℓ	landfall location in latitude and longitude

2.2 Model Simulation Setup

In this application, the ADCIRC simulator and the SWAN + ADCIRC simulator are run on the same mesh with 148,055 nodes (spatial points). The mesh and simulation characteristics were constructed for a FEMA coastal flood hazard study (FEMA, 2017) and these simulations were carried out using the same standards and methods of that study. We primarily focus on storm surges at N=9,284 spatial locations in the Cape Coral region of Southwestern Florida, since Cape Coral is a study region in the FEMA Region IV's mission, and has suffered from great storm surge damages historically. 50 unique combination of storm parameters $(\Delta P, R_p, V_f, \theta, B)$ are selected based on the maximin Latin hypercube design

(LHD) in the input domain $[30,70] \times [16,39] \times [3,10] \times [15,75] \times [0.9,1.4]$. For each combination of these 5 storm parameters, the landfall location ℓ is repeated with one R_p spacing along the coastline in Cape Coral. For each of the 5 storm parameters, the initial position of landfall location is randomly chosen, meaning that no two storms make landfall at the same location. In total, we obtained 226 inputs, which will be referred to as \mathcal{X}_0 . We randomly selected 60 inputs from the 226 inputs to run the SWAN + ADCIRC simulator, which will be referred to as \mathcal{X}_2 . Then we randomly selected 140 inputs from the the remaining 166 inputs to run the ADCIRC simulator, which will be referred to as \mathcal{X}_1^1 . To characterize the difference between the ADCIRC simulator and the SWAN + ADCIRC simulator, we also randomly chose 50 inputs form the 60 inputs to run the ADCIRC simulator, which will be referred to as \mathcal{X}_1^2 . Let $\mathcal{X}_1 := \mathcal{X}_1^1 \cup \mathcal{X}_1^2$ be the collection of 200 inputs from \mathcal{X}_1^1 and \mathcal{X}_1^2 . Notice that only 50 inputs in the SWAN + ADCIRC simulator are nested within the 200 inputs in the ADCIRC simulator. The meteorological forcing in both the ADCIRC simulator and the SWAN + ADCIRC simulator is produced by a single group (Oceanweather, Inc.) using the work in Cardone and Cox (2009).

Figure 2 shows peak surge elevations over 9, 284 spatial locations from the ADCIRC simulator and the SWAN + ADCIRC simulator at two different input settings $\mathbf{x}_1 = (48.30, 20.48, 6.187, 62.28, 1.260, -82.08, 26.59)^{\mathsf{T}}$ and $\mathbf{x}_2 = (68.85, 34.34, 8.778, 55.57, 1.066, -82.15, 26.69)^{\mathsf{T}}$. The output surfaces also have very different variations in different regions at each fidelity level. This indicates that a spatially-varying mean function or a spatially-varying variance function may help capture the spatial variations in the output space. The third column shows that PSEs have their maximum difference less than 0.3 meters between the low and high fidelity simulators, and also shows that the discrepancy has different spatial structures. At some specific regions such as the Fort Myers Beach (on the top right panel), very sharp changes can be detected. Physically, the changes in the surge elevation arise from differences in the spatial and temporal structures of the surge-only versus the wave response to storm forcing. For instance, in the top panel, the addition of wave-driven water level setup

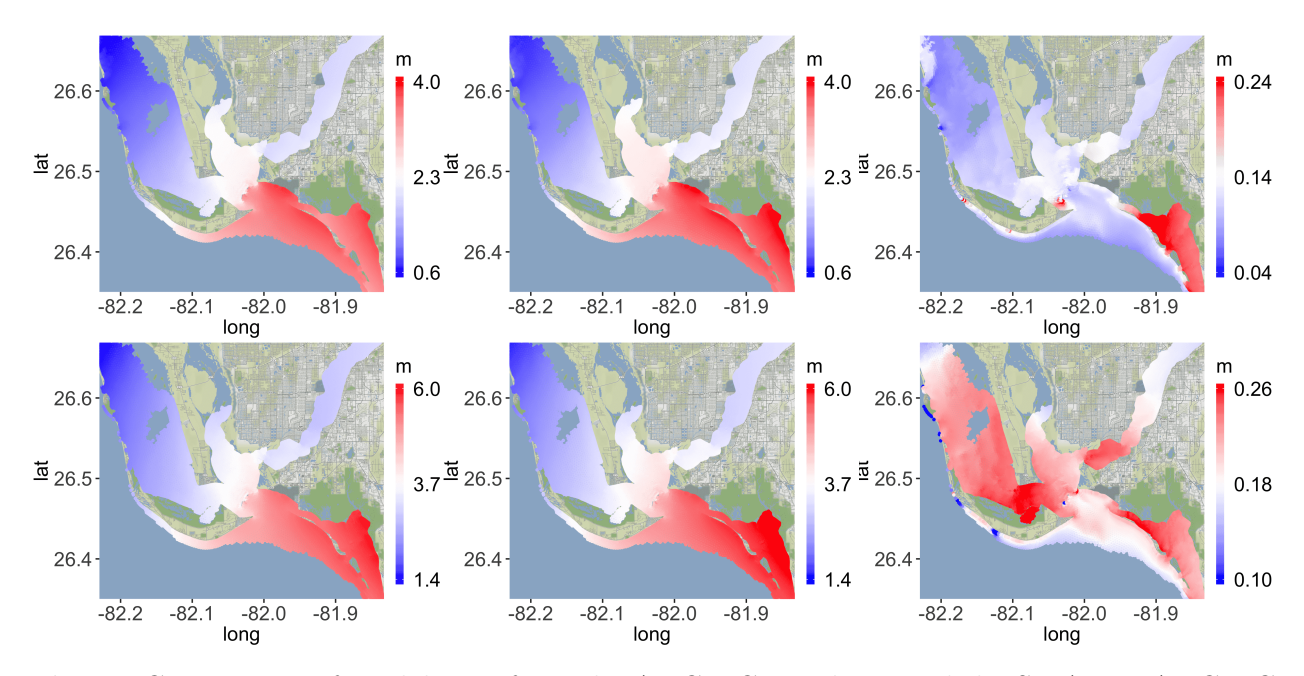


Fig. 2. Comparison of model runs from the ADCIRC simulator and the SWAN + ADCIRC simulator at two input settings. The first and second columns show the model runs from the low-fidelity simulator and the high-fidelity simulator. The third column shows the difference between the high-fidelity run and the low-fidelity run.

leads to greater overtopping (a situation when waves are higher than the dunes or structures they encounter) of coastal barrier islands, bringing greater water into the semi-protected bays in the southeastern portion of the figure. It can be difficult to detect these sorts of patterns without modeling wind-driven wave effects. Although the discrepancy between the low-fidelity simulator and high-fidelity simulator is "small", the accuracy of storm surges has a substantial impact on risk assessment of storm surges in coastal areas, and the increase in computational cost is substantial. In what follows, we develop a cokriging based emulator to approximate the high-fidelity simulator by combining simulations from a limited number of high-fidelity runs and a larger number of low-fidelity simulation runs.

3 The Methodology

3.1 A Univariate Autoregressive Cokriging Model

Assume that we have s levels of code with output functions $y_1(\cdot), \ldots, y_s(\cdot)$, where the code associated to $y_t(\cdot)$ is assumed to be more accurate than the one associated to $y_{t-1}(\cdot)$ for $t=2,\ldots,s$. Let \mathcal{X} be a compact subset of \mathbb{R}^d , which is assumed to be the input space of computer code. Further assume that the code $y_t(\cdot)$ is run at a set of input values denoted by $\mathcal{X}_t \subset \mathcal{X}$ for $t=1,\ldots,s$, where \mathcal{X}_t contains n_t input values. Consider the following autoregressive model:

$$y_t(\cdot) = \gamma_{t-1}(\cdot)y_{t-1}(\cdot) + \delta_t(\cdot), \quad t = 2, \dots, s,$$
(3.1)

where $\delta_t(\cdot)$ is the unknown location discrepancy representing the local adjustment from level t-1 to level t. Likewise, $\gamma_{t-1}(\cdot)$ is the scale discrepancy representing the scale change from level t-1 to level t. $\gamma_{t-1}(\cdot)$ can be modeled as a basis function representation, i.e., $\gamma_{t-1}(\cdot) = \mathbf{w}_{t-1}(\cdot)^{\top} \boldsymbol{\xi}_{t-1}$ for t=2,...,s where $\mathbf{w}_{t-1}(\cdot)$ is a vector of known basis functions and $\boldsymbol{\xi}_{t-1}$ is a vector of unknown coefficients.

To account for uncertainties in the unknown functions $y_1(\cdot)$ and $\delta_t(\cdot)$, we assign Gaussian process priors

$$y_1(\cdot) \mid \boldsymbol{\beta}_1, \sigma_1^2, \boldsymbol{\phi}_1 \sim \mathcal{GP}(\mathbf{h}_1^{\top}(\cdot)\boldsymbol{\beta}_1, \sigma_1^2 r(\cdot, \cdot | \boldsymbol{\phi}_1)),$$

$$\delta_t(\cdot) \sim \mathcal{GP}(\mathbf{h}_t^{\top}(\cdot)\boldsymbol{\beta}_t, \sigma_t^2 r(\cdot, \cdot | \boldsymbol{\phi}_t)),$$
(3.2)

for t = 2, ..., s. Here, $r(\cdot, \cdot \mid \boldsymbol{\phi}_t)$ is a correlation function with parameters $\boldsymbol{\phi}_t$. Following (Sacks et al., 1989), we use a product form of correlation structure, i.e., $r(\mathbf{x}, \mathbf{x}' \mid \boldsymbol{\phi}_t) = \prod_{i=1}^d r_i(x_i, x_i' \mid \boldsymbol{\phi}_{t,i})$. For each input dimension, we will focus on the Matérn family of the following form:

$$r(u \mid \phi) = \frac{2^{1-\nu}}{\Gamma(\nu)} \left(\frac{\sqrt{2\nu}u}{\phi} \right)^{\nu} \mathcal{K}_{\nu} \left(\frac{\sqrt{2\nu}u}{\phi} \right),$$

where u is the distance between two inputs along a specific input dimension. $\mathcal{K}_v(\cdot)$ is the modified Bessel function of the second kind, ϕ is a range parameter, and v is a smoothness parameter controlling the differentiability of the Gaussian process. This parameter is typically chosen to be a fixed value, since it cannot be estimated consistently based on a single realization of a Gaussian process (Stein, 1999). The choice of this parameter value is often made after a preliminary examination of the application. In our storm surge application, we have taken in to account that the underling physical process is typically smooth, and we judged that a reasonable choice for the smoothness parameter is 2.5. If a nugget term is assumed in the correlation function $r(\cdot, \cdot \mid \phi_t)$, the notation ϕ_t includes both the range parameters and the nugget parameter. $\mathbf{h}_t(\cdot)$ is a vector of basis functions and β_t is a vector of coefficients at code level t.

The autoregressive cokriging model defined in (3.1) and (3.2) has been used to model computer model output at different fidelity levels in previous work (e.g., Kennedy and O'Hagan, 2000; Qian and Wu, 2008; Le Gratiet, 2013). However, in order to be able to perform the required computations in practice, these models are built upon the assumption that the input design is hierarchically nested, in the sense that $\mathcal{X}_t \subset \mathcal{X}_{t-1}$ for t = 2, ..., s. In practice, the code may not be run at each level with a hierarchically nested design, and hence the above assumption can be an important restriction. In Figure 3, a toy example is used to illustrated the performance of autoregressive cokriging with a non-nested design. This example shows that the information from a low-fidelity code can be used to better infer the high-fidelity code. In the storm surge application, each simulator generates highly multivariate output. To the best of our knowledge, no method has been proposed to tackle this high-dimensional problem for multilevel computer models.

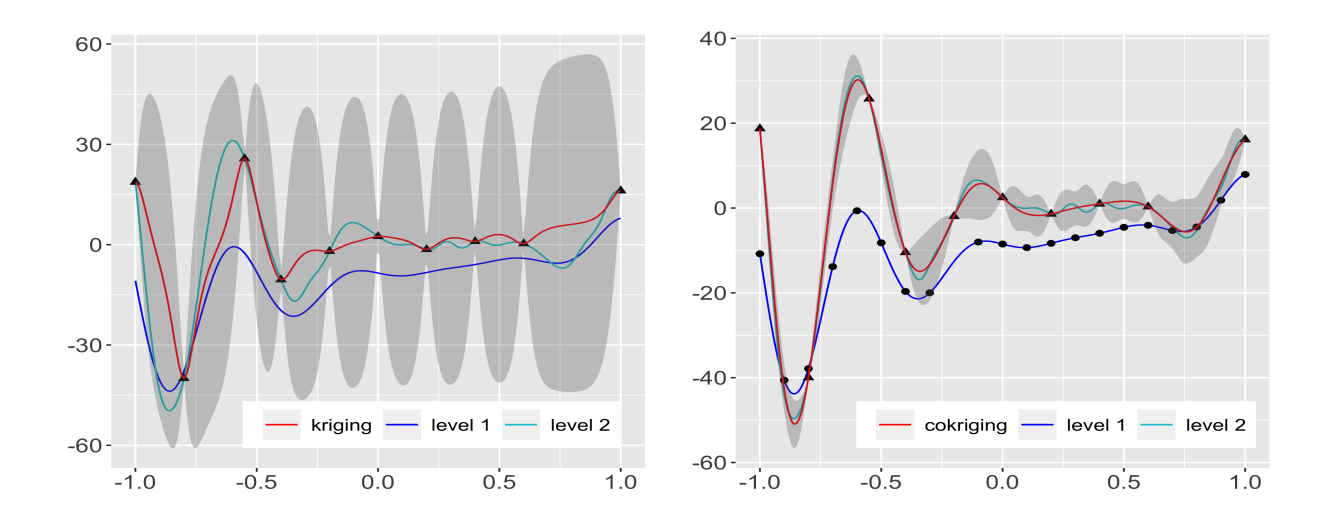


Fig. 3. Illustration of the autoregressive cokriging model under a non-nested design. The low-fidelity code is $y_1(x) = 0.5(6x - 2)^2 \sin(12x - 4) + 10(x - 0.5) - 5$, and the high-fidelity code is $y_2(x) = 2y_1(x) - 20x + 20 + \sin(10\cos(5x))$. The triangles represent design points for the high-fidelity code (level 2 code). The dots represent design points for the low-fidelity code (level 1 code). The left panel shows the kriging emulator trained against only high-fidelity runs at 10 design points via the R package RobustGaSP (Gu et al., 2018). The right panel shows the autoregressive cokriging emulator trained against both low-fidelity runs at 20 design points and high-fidelity runs at 10 design points. The bounds in gray areas are 95% credible intervals. Two design points run by the high-fidelity code are not nested within the design points run by the low-fidelity code.

3.2 Extension for High-Dimensional Output

In Section 3.1, we only consider a univariate output for the code $y_t(\cdot)$ at each fidelity level. Suppose that each level of code gives output values over the same N spatial locations, and that there are available n_t simulations of the code at different input values at level t. Let $\mathbf{y}_{t,j}$ be a vector of output values over all inputs in \mathcal{X}_t at coordinate j and code level t. Let $\mathbf{y}_{t,1}^{\mathsf{T}}, \dots, \mathbf{y}_{t,N}^{\mathsf{T}}$ be a vector of output values across all spatial locations and input values at level t. Let $\mathbf{y}_j^{\mathcal{D}} := (\mathbf{y}_{1,j}^{\mathsf{T}}, \dots, \mathbf{y}_{s,j}^{\mathsf{T}})^{\mathsf{T}}$ be a vector of output values at coordinate j over all inputs in \mathcal{X} and all code levels. Let $(\mathbf{y}_t)_{j=1}^N := (y_{t,1}, \dots, \mathbf{y}_{t,N})^{\mathsf{T}}$ be a vector of output at code level t over all N spatial coordinates.

A standard approach to dealing with multivariate output is to assume a separable covariance structure between input space and output space (Conti and O'Hagan, 2010), that is, the correlation matrix for output, $\mathbf{y}^{t,\mathscr{D}}$, is a Kronecker product of the spatial correlation matrix and the model input correlation matrix. In the storm surge application, each model run generates output at N = 9,284 spatial locations. As the number of simulator output is high-dimensional for the storm surge application and many real applications, this approach is computationally infeasible. Gu and Berger (2016) show that by assuming independent Gaussian processes for each coordinate with the same range parameter only, the parallel partial (PP) Gaussian process emulator will give identical posterior predictive mean and nearly identical posterior predictive variance as in Conti and O'Hagan (2010). However, a main limitation of this approach is the lack of joint modeling among spatial locations due to the independence assumption. In the storm surge application, the goal of obtaining the marginal distribution would suffice. This parallel partial idea is attractive when the interest is in the predictive mean and predictive variance, since the computation is linear in the number of simulator outputs N, and the computation can even be parallelized to ensure scalability for massive outputs.

In what follows, we extend the univariate formulation in Section 3.1 to multivariate

formulation using the parallel partial idea in Gu and Berger (2016).

3.2.1 The Parallel Partial Cokriging Model

For each coordinate j, we assume independent autoregressive cokriging models with different regression parameters $\{\beta_{1,j}, \ldots, \beta_{s,j}\}$, different variance parameters $\{\sigma_{1,j}^2, \ldots, \sigma_{s,j}^2\}$, different scale discrepancy parameters $\{\gamma_{1,j}, \ldots, \gamma_{t-1,j}\}$, but the same correlation parameters $\boldsymbol{\phi} := (\boldsymbol{\phi}_1, \ldots, \boldsymbol{\phi}_s)^{\top}$. For the j-th coordinate, the following cokriging model is assumed:

$$y_{t,j}(\cdot) = \gamma_{t-1,j}(\cdot)y_{t-1,j}(\cdot) + \delta_{t,j}(\cdot)$$
(3.3)

for t = 2, ..., s and j = 1, ..., N, where $y_{1,j}(\cdot)$, $\delta_{t,j}(\cdot)$ and $\gamma_{t-1,j}(\cdot)$ are unknown functions. Similar to Section 3.1, we assume $\gamma_{t-1,j}$ to be an unknown constant and assume the following Gaussian processes

$$y_{1,j}(\cdot) \mid \boldsymbol{\beta}_{1,j}, \sigma_{1,j}^{2}, \boldsymbol{\phi}_{1} \sim \mathcal{GP}(\mathbf{h}_{1}^{\top}(\cdot)\boldsymbol{\beta}_{1,j}, \sigma_{1,j}^{2}r(\cdot, \cdot|\boldsymbol{\phi}_{1})),$$

$$\delta_{t,j}(\cdot) \sim \mathcal{GP}(\mathbf{h}_{t}^{\top}(\cdot)\boldsymbol{\beta}_{t,j}, \sigma_{t,j}^{2}r(\cdot, \cdot|\boldsymbol{\phi}_{t})),$$
(3.4)

where $\mathbf{h}_t(\cdot)$ is a vector of common fixed basis functions across all N spatial locations. $\sigma_{t,j}^2$ is the variance parameters at each fidelity level and spatial location. $r(\cdot, \cdot | \phi_t)$ is a correlation function with parameters ϕ_t . If a nugget term is assumed in this correlation function, we can assume that the parameters ϕ_t include not only range parameters in a Gaussian process, but also a nugget term τ_t^2 . As in Section 3.1, one can use a product form of Matérn correlation functions.

The model developed in (3.3) and (3.4) leads to a methodology that we call parallel partial cokriging. Here the parallel partial (PP) reflects the fact that independent autoregressive cokriging models are assumed for each coordinate but they share the same correlation parameters.

3.2.2 Data Augmentation

Given the cokriging model in (3.3) and (3.4), the form of the marginal likelihood often requires that the collection of input runs at each level is nested in order to have closed-form inference, i.e., $\mathcal{X}_t \subset \mathcal{X}_{t-1}$. In this article, we develop a Bayesian approach for non-nested design, since the code run at each level does not necessarily require the inputs to be nested in practice. To present our idea, we replace original input domain \mathcal{X}_t by $\tilde{\mathcal{X}}_t = \mathcal{X}_t \cup \mathring{\mathcal{X}}_t$ such that $\mathring{\mathcal{X}}_t := \mathcal{X}_{(t+1):s} \setminus \mathcal{X}_t$, where $\mathcal{X}_{(t+1):s} := \bigcup_{k=t+1}^s \mathcal{X}_k$. Let $\mathring{\mathbf{y}}_{t,j}$ be a vector of missing output values all inputs in $\mathring{\mathcal{X}}_t$ at coordinate j and code level t. Let $\mathring{\mathbf{y}}_j^{\mathcal{Y}} := (\mathring{\mathbf{y}}_{1,j}^{\mathsf{T}}, \dots, \mathring{\mathbf{y}}_{s,j}^{\mathsf{T}})^{\mathsf{T}}$ be a vector of missing output values at coordinate j over all inputs in $\mathring{\mathcal{X}}_t$ and all code levels, where $\mathring{\mathbf{y}}_{s,j}^{\mathsf{T}}$ is defined to be empty for notational convenience. Let $(\mathring{\mathbf{y}}_t)_{j=1}^N := (\mathring{\mathbf{y}}_{t,1}^{\mathsf{T}}, \dots, \mathring{\mathbf{y}}_{t,N}^{\mathsf{T}})^{\mathsf{T}}$ be a vector of missing output at code level t over all N spatial coordinates. Let $\tilde{\mathbf{y}}_{t,j} := (\mathbf{y}_{t,j}^{\mathsf{T}}, \mathring{\mathbf{y}}_{t,j}^{\mathsf{T}})^{\mathsf{T}}$ and $\tilde{\mathbf{y}}_j^{\mathcal{Y}} := (\mathbf{y}_j^{\mathsf{T}}, \mathring{\mathbf{y}}_j^{\mathsf{T}})^{\mathsf{T}}$. Then the augmented sampling distribution at the j-th coordinate is

$$L(\tilde{\mathbf{y}}_{j}^{\mathscr{D}} \mid \boldsymbol{\beta}_{j}, \boldsymbol{\gamma}_{j}, \boldsymbol{\sigma}_{j}^{2}, \boldsymbol{\phi}) \propto \pi(\tilde{\mathbf{y}}_{1,j} \mid \boldsymbol{\beta}_{1,j}, \sigma_{1,j}^{2}, \boldsymbol{\phi}_{1}) \prod_{t=2}^{s} \pi(\tilde{\mathbf{y}}_{t,j} \mid \boldsymbol{\beta}_{t,j}, \gamma_{t,j}, \sigma_{t,j}^{2}, \boldsymbol{\phi}_{t}),$$
(3.5)

with

$$\begin{split} \pi(\tilde{\mathbf{y}}_{1,j} \mid \boldsymbol{\beta}_{1,j}, \sigma_{1,j}^2, \boldsymbol{\phi}_1) &= \mathcal{N}(\tilde{\mathbf{H}}_1 \boldsymbol{\beta}_{1,j}, \sigma_{t,j}^2 \tilde{\mathbf{R}}_1), \\ \pi(\tilde{\mathbf{y}}_{t,j} \mid \boldsymbol{\beta}_{t,j}, \gamma_{t,j}, \sigma_{t,j}^2, \boldsymbol{\phi}_t) &= \mathcal{N}(\tilde{\mathbf{H}}_{1,j} \boldsymbol{\beta}_{1,j} + \tilde{W}_{t-1,j} \gamma_{t-1,j}, \sigma_{t,j}^2 \tilde{\mathbf{R}}_t), \end{split}$$

where $\tilde{\mathbf{H}}_{t,j} := \mathbf{h}_t(\tilde{\mathcal{X}}_t)$, $\tilde{\mathbf{R}}_t := r(\tilde{\mathcal{X}}_t, \tilde{\mathcal{X}}_t \mid \boldsymbol{\phi}_t)$, and $\tilde{W}_{t-1,j} := \mathbf{y}_{t-1,j}(\tilde{\mathcal{X}}_t)$ with $y_{t-1,j}(A) := [y_{t-1,j}(\mathbf{x}), \mathbf{x} \in A]$ being a vector of output over inputs in A. When A is either \mathcal{X}_t or $\mathring{\mathcal{X}}_t$, it follows immediately that $y_{t-1,j}(\mathcal{X}_t) = y_{t-1,j}(\mathcal{X}_t \cap \mathring{\mathcal{X}}_{t-1})$ and $y_{t-1,j}(\mathring{\mathcal{X}}_t) = y_{t-1,j}(\mathring{\mathcal{X}}_t \cap \mathring{\mathcal{X}}_{t-1})$ which are both sub-vectors of $\mathring{\mathbf{y}}_{t-1,j}$, since $\mathcal{X}_t \subset \mathring{\mathcal{X}}_{t-1}$ and $\mathring{\mathcal{X}}_t \subset \mathring{\mathcal{X}}_{t-1}$. This sampling distribution provides a convenient form to perform likelihood-based inference.

3.2.3 Parameter Estimation

Let $\tilde{\mathbf{y}}^{\mathscr{D}} := (\tilde{\mathbf{y}}_1^{\mathscr{D}^{\top}}, \dots, \tilde{\mathbf{y}}_N^{\mathscr{D}^{\top}})^{\top}$ be a vector of augmented outputs over all N spatial locations. We introduce the following notation: $\boldsymbol{\beta} := (\boldsymbol{\beta}_1^{\top}, \dots, \boldsymbol{\beta}_N^{\top})^{\top}$, $\boldsymbol{\gamma} := (\boldsymbol{\gamma}_1^{\top}, \dots, \boldsymbol{\gamma}_N^{\top})^{\top}$, and $\boldsymbol{\sigma}^2 := (\boldsymbol{\sigma}_1^{2\top}, \dots, \boldsymbol{\sigma}_N^{2\top})^{\top}$. The overall augmented sampling distribution across all N spatial locations is assumed to be a product of each augmented sampling distribution, which is given by

$$L(\tilde{\mathbf{y}}^{\mathscr{D}} \mid \boldsymbol{\beta}, \boldsymbol{\gamma}, \boldsymbol{\sigma}^{2}, \boldsymbol{\phi}) = \prod_{j=1}^{N} L(\tilde{\mathbf{y}}_{j}^{\mathscr{D}} \mid \boldsymbol{\beta}_{j}, \boldsymbol{\gamma}_{j}, \boldsymbol{\sigma}_{j}^{2}, \boldsymbol{\phi}).$$
(3.6)

We specify the following a priori model for the unknown parameters

$$\pi(\boldsymbol{\beta}, \boldsymbol{\gamma}, \boldsymbol{\sigma}^2, \boldsymbol{\phi}) = \pi(\boldsymbol{\beta}, \boldsymbol{\gamma}, \boldsymbol{\sigma}^2) \pi(\boldsymbol{\phi}) = \pi(\boldsymbol{\phi}) \prod_{j=1}^{N} \left\{ \pi(\boldsymbol{\beta}_{s,j}, \sigma_{s,j}^2) \prod_{t=1}^{s-1} \pi(\boldsymbol{\beta}_{t,j}, \gamma_{t,j}, \sigma_{t,j}^2) \right\}, \quad (3.7)$$

where independent Jeffreys prior can be assumed for $\beta_{t,j}$, $\gamma_{t-1,j}$, $\sigma_{t,j}^2$: i.e., $\pi(\beta_{t,j}, \gamma_{t-1,j}, \sigma_{t,j}^2) \propto \frac{1}{\sigma_{t,j}^2}$ for $t = 2, \ldots, s$, and $\pi(\beta_{1,j}, \sigma_{1,j}^2) \propto \frac{1}{\sigma_{1,j}^2}$ at each coordinate j. For each level t, the jointly robust prior (Gu, 2019) is assumed for ϕ_t . The jointly robust prior is a proper prior and has been shown to have desirable properties for Gaussian process emulation.

After integrating out model parameters $\{\beta, \gamma, \sigma^2\}$, the conditional distribution of $\tilde{\mathbf{y}}^{\mathscr{D}}$ given $\boldsymbol{\phi}$ is

$$\pi(\tilde{\mathbf{y}}^{\mathscr{D}} \mid \boldsymbol{\phi}) = \prod_{j=1}^{N} \pi(\tilde{\mathbf{y}}_{1,j} \mid \boldsymbol{\phi}_1) \prod_{t=2}^{s} \pi(\tilde{\mathbf{y}}_{t,j} \mid \boldsymbol{\phi}_t, \tilde{\mathbf{y}}_{t-1,j}), \tag{3.8}$$

with $\pi(\tilde{\mathbf{y}}_{t,j} \mid \boldsymbol{\phi}_t, \tilde{\mathbf{y}}_{t-1,j}) \propto |\tilde{\mathbf{R}}_t|^{-1/2} |\tilde{\mathbf{T}}_{t,j}^{\top} \tilde{\mathbf{R}}_t^{-1} \tilde{\mathbf{T}}_{t,j}|^{-1/2} \{ S^2(\boldsymbol{\phi}_t, \tilde{\mathbf{y}}_{t,j}) \}^{-(\tilde{n}_t - q_t)/2}, \text{ where } \tilde{\mathbf{T}}_{1,j} = \tilde{\mathbf{H}}_1$ for $j = 1, \dots, N$ and $\tilde{\mathbf{T}}_{t,j} = [\tilde{\mathbf{H}}_t, \tilde{W}_{t-1,j}]$ for $t = 2, \dots, s$ and $j = 1, \dots, N$. $S^2(\boldsymbol{\phi}_t, \tilde{\mathbf{y}}_{t,j}) := \tilde{\mathbf{y}}_{t,j}^{\top} \tilde{\mathbf{Q}}_t \tilde{\mathbf{y}}_{t,j}$ with $\tilde{\mathbf{Q}}_t := \tilde{\mathbf{R}}_t^{-1} \{ \mathbf{I} - \tilde{\mathbf{T}}_{t,j} (\tilde{\mathbf{T}}_{t,j}^{\top} \tilde{\mathbf{R}}_t^{-1} \tilde{\mathbf{T}}_{t,j})^{-1} \tilde{\mathbf{T}}_{t,j}^{\top} \tilde{\mathbf{R}}_t^{-1} \}.$

To estimate ϕ , we take an empirical Bayesian approach to maximizing the integrated posterior $\pi(\phi \mid \tilde{\mathbf{y}}^{\mathscr{D}})$, since the empirical Bayesian approach has the advantage of avoiding Markov chain Monte Carlo methods and is computationally faster than the fully Bayesian approach. As direct maximization of $\pi(\phi \mid \tilde{\mathbf{y}}^{\mathscr{D}})$ is impossible due to the intractable form of $\pi(\phi \mid \tilde{\mathbf{y}}^{\mathscr{D}})$, we introduce an expectation-maximization (EM) algorithm to tackle this

challenge. In the EM algorithm, we treat $\mathring{\mathbf{y}}^{\mathscr{D}}$ as "missing data" and $\{\mathring{\mathbf{y}}^{\mathscr{D}}, \mathbf{y}^{\mathscr{D}}\}$ as the complete data. Let $\boldsymbol{\phi}^{[\ell]}$ be the parameters in the ℓ th iteration of the EM algorithm. The EM algorithm consists of two steps. The first step is to compute the so-called Q-function based on a complete-data-log-likelihood $\ln \pi(\tilde{\mathbf{y}}^{\mathscr{D}}, \boldsymbol{\phi})$ in the E-step, which is given by

$$\ln \pi(\tilde{\mathbf{y}}^{\mathscr{D}}, \boldsymbol{\phi}) = \sum_{t=1}^{s} g_t(\boldsymbol{\phi}_t, (\mathring{\mathbf{y}}_t)_{j=1}^N), \tag{3.9}$$

where $(\mathring{\mathbf{y}}_t)_{j=1}^N := (\mathring{\mathbf{y}}_{t,1}, \dots, \mathring{\mathbf{y}}_{t,N})^{\top}$ and $g_t(\boldsymbol{\phi}_t, (\mathring{\mathbf{y}}_t)_{j=1}^N) := -N \ln |\tilde{\mathbf{R}}_t|/2 - \sum_{j=1}^N \ln |\tilde{\mathbf{T}}_{t,j}^{\top} \tilde{\mathbf{R}}_t^{-1} \tilde{\mathbf{T}}_{t,j}|/2 - (\tilde{n}_t - q_t) \sum_{j=1}^N \ln S^2(\boldsymbol{\phi}_t, \mathring{\mathbf{y}}_{t,j})/2 + \ln \pi(\boldsymbol{\phi}_t).$

Starting with initial values $\phi^{[\ell]}$ at the ℓ -th iteration, we compute the Q-function in the E-step: $Q(\phi; \phi^{[\ell]}) = E_{\pi(\mathring{\mathbf{y}}^{\mathscr{D}}|\mathbf{y}^{\mathscr{D}}, \phi^{[\ell]})}\{\ln \pi(\widetilde{\mathbf{y}}^{\mathscr{D}}, \phi)\}$, where the conditional distribution $\pi(\mathring{\mathbf{y}}^{\mathscr{D}} \mid \mathbf{y}^{\mathscr{D}}, \phi^{[\ell]})$ is given in Appendix B. As this expectation cannot be computed analytically, Monte Carlo samples from the distribution $\pi(\mathring{\mathbf{y}}^{\mathscr{D}} \mid \mathbf{y}^{\mathscr{D}}, \phi^{[\ell]})$ can be used to approximate this expectation. Specifically, the Q-function is

$$Q(\boldsymbol{\phi}; \boldsymbol{\phi}^{[\ell]}) \approx \sum_{t=1}^{s} \underbrace{\frac{1}{M} \sum_{k=1}^{M} g_t(\boldsymbol{\phi}_t, (\mathring{\mathbf{y}}_t^{[k]})_{j=1}^N)}_{=\hat{Q}_{t,M}(\boldsymbol{\phi}_t | \boldsymbol{\phi}_t^{[\ell]})}, \tag{3.10}$$

where $\{(\mathring{\mathbf{y}}_t^{[k]})_{j=1}^N: t=1,\ldots,s\}$ is a sample from the distribution $\pi(\mathring{\mathbf{y}}^{\mathscr{D}}\mid \mathbf{y}^{\mathscr{D}}, \boldsymbol{\phi}^{[\ell]})$. The second step is to numerically maximize this function with respect to parameters $\boldsymbol{\phi}_t$ for $t=1,\ldots,s$. This leads to the so-called Monte Carlo EM (MCEM) algorithm (Wei and Tanner, 1990).

In each iteration of the MCEM algorithm, the computation of the function $g(\phi_t, (\mathring{\mathbf{y}}_t)_{j=1}^N)$ has computational cost $O(N\tilde{n}_t^3)$. Lemma 2 in Appendix A shows that the computational complexity of this function can be reduced to $O(N\tilde{n}_t^2 + \tilde{n}_t^3)$, which substantially reduces computational cost when N is very large as in our real application. In addition, parameters $\{\phi_t: t=1,\ldots,s\}$ can be estimated independently in the M-step. This allows great advantage in estimating model parameters with the proposed methodology. As the number of simulations is limited for high-fidelity simulators in real applications, the proposed cokriging

model is anticipated to produce more stable estimates than independent kriging models. The procedure of the MCEM algorithm is given in Algorithm 1.

Algorithm 1 The MCEM algorithm

Input: Initial values $\phi^{[1]}$, data \mathbf{y} and $\ell = 1$.

Output: Values ϕ that maximize $\pi(\phi \mid \mathbf{y})$.

1: repeat

2: Generate M samples from $\pi(\mathring{\mathbf{y}}^{\mathscr{D}} \mid \mathbf{y}^{\mathscr{D}}, \boldsymbol{\phi}^{[\ell]})$, which are denoted by $\{(\mathring{\mathbf{y}}_t^{[k]})_{j=1}^N : t = 1, \ldots, s; k = 1, \ldots, M\}$.

3: **for** t = 1, ..., s **do**

⊳ can be run in parallel

4: E-step:

$$\hat{Q}_{t,M}(\phi_t \mid \phi_t^{[\ell]}) = \frac{1}{M} \sum_{k=1}^{M} g_t(\phi_t, (\mathring{\mathbf{y}}_t^{[k]})_{j=1}^N).$$

5: M-step:

$$oldsymbol{\phi}_t^{[\ell+1]} := rg \max_{oldsymbol{\phi}_t} \hat{Q}_{t,M}(oldsymbol{\phi}_t \mid oldsymbol{\phi}_t^{[\ell]}).$$

6: end for

7: **until** certain stopping convergence criterion is satisfied.

3.2.4 Prediction

For any new input $\mathbf{x}_0 \in \mathcal{X}$, the goal is to make prediction for $\{y_{s,j}(\mathbf{x}_0), j = 1, \dots, N\}$ based upon the data $\mathbf{y}^{\mathscr{D}}$. With the prior model (3.7), the predictive distribution of interest is $y_{s,j}(\mathbf{x}_0 \mid \mathbf{y}^{\mathscr{D}}, \boldsymbol{\phi})$ for $j = 1, \dots, N$.

In what follows, we derive the predictive distribution in two different ways. The first approach is based on the same idea used in Kennedy and O'Hagan (2000); Le Gratiet (2013). It is easy to show that

$$\pi(\mathbf{y}_s(\mathbf{x}_0) \mid \mathbf{y}^{\mathscr{D}}, \boldsymbol{\phi}) = \prod_{j=1}^N \int \pi(y_{s,j}(\mathbf{x}_0) \mid \mathbf{y}_j^{\mathscr{D}}, \boldsymbol{\beta}_j, \boldsymbol{\gamma}_j, \boldsymbol{\sigma}_j^2, \boldsymbol{\phi}) \pi(\boldsymbol{\beta}_j, \boldsymbol{\gamma}_j, \boldsymbol{\sigma}_j^2) d\{\boldsymbol{\beta}_j, \boldsymbol{\gamma}_j, \boldsymbol{\sigma}_j^2\}.$$

Notice that

$$\pi(y_{s,j}(\mathbf{x}_0) \mid \mathbf{y}_j^{\mathscr{D}}, \boldsymbol{\beta}_j, \boldsymbol{\gamma}_j, \boldsymbol{\sigma}_j^2, \boldsymbol{\phi}) = \int \pi(y_{s,j}(\mathbf{x}_0) \mid \tilde{\mathbf{y}}_j^{\mathscr{D}}, \boldsymbol{\beta}_j, \boldsymbol{\gamma}_j, \boldsymbol{\sigma}_j^2, \boldsymbol{\phi}) \times \pi(\mathring{\mathbf{y}}_j^{\mathscr{D}} \mid \mathbf{y}_j^{\mathscr{D}}, \boldsymbol{\beta}_j, \boldsymbol{\gamma}_j, \boldsymbol{\sigma}_j^2, \boldsymbol{\phi}) d\{\mathring{\mathbf{y}}_j^{\mathscr{D}}\}$$

$$(3.11)$$

where $\pi(\mathring{\mathbf{y}}_j^{\mathscr{D}} \mid \mathbf{y}_j^{\mathscr{D}}, \boldsymbol{\beta}_j, \boldsymbol{\gamma}_j, \boldsymbol{\sigma}_j^2, \boldsymbol{\phi})$ is a multivariate normal distribution with mean and variance given in Appendix B. $\pi(y_{s,j}(\mathbf{x}_0) \mid \tilde{\mathbf{y}}_j, \boldsymbol{\beta}_j, \boldsymbol{\gamma}_j, \boldsymbol{\sigma}_j^2, \boldsymbol{\phi})$ is a normal distribution with mean $m_{s,j}(\mathbf{x}_0)$ and variance $v_{s,j}(\mathbf{x}_0)$ given in Lemma 1 of Appendix A, which requires $O(N(\sum_{t=1}^s \tilde{n}_t)^3)$ flops to compute for all spatial locations. In the storm surge application, the high-dimentionality of simulator output makes this predictive formula computationally infeasible. In addition, to obtain predictive distribution $\pi(y_{s,j}(\mathbf{x}_0) \mid \mathbf{y}^{\mathscr{D}}, \boldsymbol{\phi})$, model parameters $\{\boldsymbol{\beta}, \boldsymbol{\gamma}, \boldsymbol{\sigma}^2\}$ have to be numerically integrated out, since $\pi(\mathbf{y}_s(\mathbf{x}_0) \mid \tilde{\mathbf{y}}^{\mathscr{D}}, \boldsymbol{\phi}) = \int \pi(\mathbf{y}_s(\mathbf{x}_0) \mid \tilde{\mathbf{y}}^{\mathscr{D}}, \boldsymbol{\phi}) \pi(\boldsymbol{\beta}, \boldsymbol{\gamma}, \boldsymbol{\sigma}^2) d\{\boldsymbol{\beta}, \boldsymbol{\gamma}, \boldsymbol{\sigma}^2\}$ is not available in a closed-form. This one-step predictive formula requires Monte Carlo approximations to take account of uncertainty in both model parameters $\{\boldsymbol{\beta}, \boldsymbol{\gamma}, \boldsymbol{\sigma}^2\}$ and missing data $\mathring{\mathbf{y}}^{\mathscr{D}}$. This will even hinder the practicality of this predictive formula. To overcome this challenge, we develop a sequential prediction formula. This approach gives a new way to make prediction directly without Monte Carlo approximations to integrate model parameters $\{\boldsymbol{\beta}, \boldsymbol{\gamma}, \boldsymbol{\sigma}^2\}$.

The second approach to predict $y_{s,j}(\mathbf{x}_0)$ is derived based upon the idea that the new input \mathbf{x}_0 is added to each $\mathring{\mathcal{X}}_t$ such that a hierarchical nested design can be obtained. To fix the notation, we define $\mathring{\mathcal{X}}_t^0 := \mathring{\mathcal{X}}_t \cup \{\mathbf{x}_0\}$, and $\tilde{\mathcal{X}}_t^0 := \mathcal{X}_t \cup \mathring{\mathcal{X}}_t^0$. Hence the collection of inputs $\{\tilde{\mathcal{X}}_t^0 : t = 1, \dots, s\}$ also forms a nested design with $\tilde{\mathcal{X}}_t^0 \subset \tilde{\mathcal{X}}_{t-1}^0$. Let $\mathbf{y}(\mathbf{x}_0) := (\mathbf{y}_1(\mathbf{x}_0)^\top, \dots, \mathbf{y}_s(\mathbf{x}_0)^\top)^\top$ with $\mathbf{y}_j(\mathbf{x}_0) := (y_{1,j}(\mathbf{x}_0), \dots, y_{s,j}(\mathbf{x}_0))^\top$. The predictive distribution of $\mathbf{y}(\mathbf{x}_0)$ given $\tilde{\mathbf{y}}^{\mathscr{D}}$ and $\boldsymbol{\phi}$ is the product of N independent distributions with

$$\pi(\mathbf{y}(\mathbf{x}_0) \mid \tilde{\mathbf{y}}^{\mathscr{D}}, \boldsymbol{\phi}) = \prod_{j=1}^N \pi(\mathbf{y}_j(\mathbf{x}_0) \mid \tilde{\mathbf{y}}_j^{\mathscr{D}}, \boldsymbol{\phi}).$$

The following theorem gives the predictive distribution at each spatial coordinate.

Theorem 1 (Sequential Prediction). According to the cokriging model (3.2), the predic-

tive distribution at each spatial coordinate is

$$\pi(\mathbf{y}_{j}(\mathbf{x}_{0}) \mid \tilde{\mathbf{y}}_{j}^{\mathscr{D}}, \boldsymbol{\phi}) = \pi(y_{1,j}(\mathbf{x}_{0}) \mid \tilde{\mathbf{y}}_{1,j}, \boldsymbol{\phi}_{1}) \prod_{t=2}^{s-1} \pi(y_{t,j}(\mathbf{x}_{0}) \mid \tilde{\mathbf{y}}_{t-1,j}, y_{t-1,j}(\mathbf{x}_{0}), \tilde{\mathbf{y}}_{t,j}, \boldsymbol{\phi}_{t})$$

$$\times \pi(y_{s,j}(\mathbf{x}_{0}) \mid y_{s-1,j}(\mathbf{x}_{0}), \mathbf{y}_{s,j}, \boldsymbol{\phi}_{s}).$$

$$(3.12)$$

With non-informative priors (3.7), the conditional distributions on the right-hand side of (3.12) are Student-t distributions with degrees of freedom, location, and scale parameters given by

$$\nu_{t,j} := n_t - q_t,$$

$$\boldsymbol{\mu}_{t,j} := \mathbf{T}(\mathbf{x}_0)\hat{\mathbf{b}}_{t,j} + \mathbf{r}_t^{\top}(\mathbf{x}_0)\tilde{\mathbf{R}}_t^{-1}(\tilde{\mathbf{y}}_{t,j} - \tilde{\mathbf{T}}_{t,j}\hat{\mathbf{b}}_{t,j}),$$

$$V_{t,j} := \frac{S^2(\boldsymbol{\phi}_t, \tilde{\mathbf{y}}_{t,j})}{n_t - q_t}c_{t,j}(\mathbf{x}_0),$$

$$with \ \hat{\mathbf{b}}_{t,j} := (\tilde{\mathbf{T}}_{t,j}^{\top}\tilde{\mathbf{R}}_t^{-1}\tilde{\mathbf{T}}_{t,j})^{-1}\tilde{\mathbf{T}}_{t,j}^{\top}\tilde{\mathbf{R}}_t^{-1}\tilde{\mathbf{y}}_{t,j}, S^2(\boldsymbol{\phi}_t, \tilde{\mathbf{y}}_{t,j}) := \tilde{\mathbf{y}}_{t,j}^{\top}\tilde{\mathbf{Q}}_t\tilde{\mathbf{y}}_{t,j},$$

$$c_{t,j}(\mathbf{x}_0) := r(\mathbf{x}_0, \mathbf{x}_0 | \boldsymbol{\phi}_t) - \mathbf{r}_t^{\top}(\mathbf{x}_0)\tilde{\mathbf{R}}_t^{-1}\mathbf{r}_t(\mathbf{x}_0)$$

$$+ [\mathbf{T}_{t,j}(\mathbf{x}_0) - \tilde{\mathbf{T}}_{t,j}^{\top}\tilde{\mathbf{R}}_t^{-1}\mathbf{r}_t(\mathbf{x}_0)]^{\top}(\tilde{\mathbf{T}}_{t,j}^{\top}\tilde{\mathbf{R}}_t^{-1}\tilde{\mathbf{T}}_{t,j})^{-1}[\mathbf{T}_{t,j}(\mathbf{x}_0) - \tilde{\mathbf{T}}_{t,j}^{\top}\tilde{\mathbf{R}}_t^{-1}\mathbf{r}_t(\mathbf{x}_0)],$$

$$where \ \mathbf{r}_t(\mathbf{x}_0) := r(\tilde{\mathcal{X}}_t, \mathbf{x}_0 | \boldsymbol{\phi}_t) \ and \ \mathbf{T}_{t,j}(\mathbf{x}_0) = [\mathbf{h}_t(\mathbf{x}_0), y_{t-1,j}(\mathbf{x}_0)].$$

Proof. Proof of this theorem follows straightforwardly from standard kriging results. \Box

This result shows that a random sample from the predictive distribution can be sequentially drawn from a collection of conditional distributions in an efficient manner, since the total computational cost required for such a simulation is $O(\sum_{t=1}^s \tilde{n}_t^3)$ at each spatial coordinate. As the correlation matrix is the same across all spatial locations at each fidelity level, the total computational cost to obtain one single random sample from the predictive distribution across all spatial locations is $O(\sum_{t=1}^s \tilde{n}_t^3 + N \sum_{t=1}^s \tilde{n}_t^2)$. Notice that a sample from $\pi(\mathbf{y}_s(\mathbf{x}_0) \mid \mathbf{y}^{\mathscr{D}}, \boldsymbol{\phi})$ can be obtained via the composition sample technique based on $\pi(\mathbf{y}_s(\mathbf{x}_0) \mid \mathbf{y}^{\mathscr{D}}, \boldsymbol{\phi}) = \int \pi(\mathbf{y}_s(\mathbf{x}_0) \mid \tilde{\mathbf{y}}^{\mathscr{D}}, \boldsymbol{\phi}) \pi(\mathring{\mathbf{y}}^{\mathscr{D}} \mid \mathbf{y}^{\mathscr{D}}, \boldsymbol{\phi}) \, d\mathring{\mathbf{y}}^{\mathscr{D}}$, by recycling the realizations of $\mathring{\mathbf{y}}^{\mathscr{D}}$ from Algorithm 1.

3.2.5 Computational Cost

In the PP cokriging model, the computational cost can be broken into two parts; one related to the parameter estimation and the other related to the prediction.

- In parameter estimation, each iteration of the MCEM algorithm requires the computation of $\hat{Q}_{t,M}(\phi_t \mid \phi_t^{[\ell]})$ and its numerical optimization with respect to correlation parameters ϕ_t at each level of code. The evaluation of $\hat{Q}_{t,M}(\phi_t \mid \phi_t^{[\ell]})$ requires computations of $\tilde{\mathbf{R}}_t^{-1}$, $\tilde{\mathbf{R}}_t^{-1}\tilde{\mathbf{T}}_{t,j}$, and $(\tilde{\mathbf{T}}_{t,j}^T\tilde{\mathbf{R}}_{t,j}^{-1}\tilde{\mathbf{T}}_{t,j})^{-1}$. At code level t, such an evaluation requires $O(MN\tilde{n}_t^2 + \tilde{n}_t^3)$ computational cost. If the numerical optimization requires k evaluations of $\hat{Q}_{t,M}(\phi_t \mid \phi_t^{[\ell]})$ to find the optimal value, the overall computational cost in each iteration of the MCEM algorithm is $O(kMN\sum_{t=1}^s \tilde{n}_t^2 + k\sum_{t=1}^s \tilde{n}_t^3)$ without any parallelization. This is a one-time computational cost.
- In the predictive distribution (3.12), each conditional distribution requires evaluation of $\tilde{\mathbf{R}}_t^{-1}$, $\tilde{\mathbf{T}}_{t,j}^{\top} \tilde{\mathbf{R}}_t^{-1}$, and $(\tilde{\mathbf{T}}_{t,j}^{\top} \tilde{\mathbf{R}}_{t,j}^{-1} \tilde{\mathbf{T}}_{t,j})^{-1}$. This requires $O(\tilde{n}_t^3 + N \tilde{n}_t^2)$ computational cost. One random sample generated from the predictive distribution at one new input value requires $O(\sum_{t=1}^s \tilde{n}_t^3 + N \sum_{t=1}^s \tilde{n}_t^2)$ computational cost. As \tilde{n}_t is typically small (a few hundreds at most) in many real applications, the computational cost in prediction is linear in the number of spatial locations. This indicates the scalability of the proposed method to handle high-dimensional output in multifidelity computer models.

4 Analysis of Storm Surge Simulations

In this section, the parallel partial cokriging model is used to analyze high-dimensional output from the ADCIRC simulator and the SWAN + ADCIRC simulator.

The analysis of emulation results and numerical comparison is presented to illustrate the advantage of the parallel partial cokriging model with high-dimensional output. The PP cokriging model is trained on 200 inputs from the ADCIRC simulator and 60 inputs from

the SWAN + ADCIRC simulator, where 50 inputs from the second fidelity level are nested within the first fidelity level. With such model runs, the proposed method can be applied readily. To measure predictive performance, we run the SWAN + ADCIRC simulator at 166 inputs from the original 226 inputs after excluding 60 inputs that are used in the training data.

As a comparison, we also train the parallel partial (PP) Gaussian process emulator via the R package RobustGaSP with the same 60 high-fidelity runs used in the PP cokriging emulator. As the landfall location is along the coastline, we define a distance measure d_{ℓ} to replace the actual longitude and latitude coordinate of the landfall location. Specifically, we first choose a reference location ℓ_0 to be the landfall location that is in the most northwest direction along the coastline. Then for any landfall location ℓ , d_{ℓ} is defined as the the spherical distance between ℓ and ℓ_0 . As the coastline is unique, the landfall location determines the distance measure d_{ℓ} and vice versa. In the implementation of the PP emulator and the PP cokriging model, the input variables are ΔP , R_p , V_f , θ , B, d_{ℓ} . To measure the predictive performance, we run the high-fidelity simulator at 60 new inputs that are not in the training inputs. Evaluation of predictive performance is based on root-mean-squared-prediction errors (RMSPE), coverage probability of the 95% equal-tail credible interval (CVG(95%)), average length of the 95% equal-tail credible interval (ALCI(95%)), and continuous rank probability score (CRPS; Gneiting and Raftery, 2007).

4.1 Emulation Accuracy

In the cokriging model, we include unknown constants in the mean functions. The discrepancy function is assumed to be an unknown constant as well. For parameter estimation, the MCEM algorithm is initialized with multiple starting values and took about 5 hours to achieve convergence for a pre-specified tolerance on a 2-core Macbook Pro with 8 GB random access memory. The estimated range parameters show that the peak surge elevation

is highly dependent on the inputs: central pressure deficit (ΔP) , Holland's B parameter (B), since these two inputs have relatively large range parameters compared to their input ranges in the training sets. The small impact of the landfall location (ℓ) is due to our focus on a small coastal region in Cape Coral.

In terms of prediction, the predictive mean and predictive variance is approximated by 30 random draws from the distribution (3.12). Negligible improvement is seen from increasing the number of draws. The results in Table 2 show that the PP cokriging model gives better prediction results than the PP emulator, since the PP cokriging model gives smaller RMSPE and CRPS than the PP emulator, and the PP cokriging model has nominal coverage probability close to 0.95 and short interval length for the 95% credible interval. As the root-mean-squared difference between the low-fidelity simulator runs and the highfidelity simulator runs is 0.132, the PP cokriging model gives a much smaller RMSPE that the low-fidelity simulator. Figure 4 shows the predicted PSE with the PP cokriging model against held-out PSE at two different storm inputs. This indicates a very good fit, since the predicted PSE against the held-out PSE are scattered around the 45 degree straight line. In contrast, the PP emulator is not able to provide better results than the low-fidelity simulator itself. This is mainly because the PP emulator is trained based on 60 high-fidelity simulator runs, which have limited ability to explore the complex input space. The computation of predictive means and predictive variances over N = 9,284 spatial locations at one input took about 10 seconds. This shows the computational efficiency of the PP cokriging model.

In addition, we can compute the Nash-Sutcliffe model efficiency coefficient (NSME):

NSME := 1 -
$$\frac{\sum_{j=1}^{N} \sum_{\mathbf{x} \in A} \{m_j(\mathbf{x}) - y_{2,j}(\mathbf{x})\}^2}{\sum_{j=1}^{N} \sum_{\mathbf{x} \in A} \{m_j(\mathbf{x}) - \bar{y}_{2,j}\}^2},$$

where $m_j(\mathbf{x})$ is the value to predict the high level code $y_{2,j}(\cdot)$ at input \mathbf{x} and j-th spatial coordinate and $\bar{y}_{2,j} := \sum_{\mathbf{x} \in \mathcal{X}_2} y_{2,j}(\mathbf{x})/n_2$ is the average of code $y_{2,j}(\cdot)$ at j-th spatial coordinate. The NSME computes the residual variance with the total variance. The closer NSME is to 1, the more accurate the model is. If the ADCIRC simulator is used to predict the SWAN

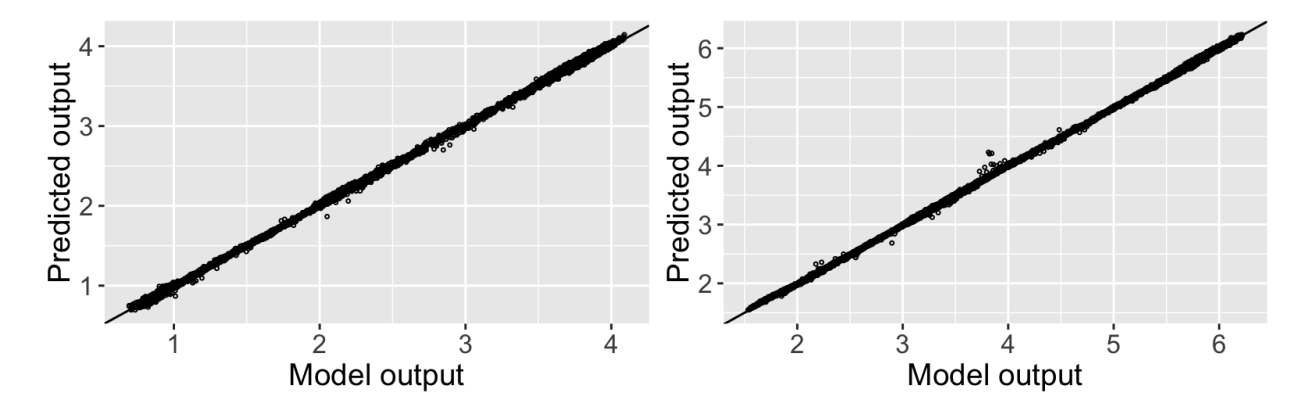


Fig. 4. Scatter plot of predicted PSE against held-out PSE over N = 9,284 spatial locations at two different input settings.

+ ADCIRC simulator at these 166 inputs, NSME is -1.089, which indicates that the mean of the training data in the high-fidelity simulator is a better predictor than the low-fidelity simulator at these inputs. The PP emulator has NSME -1.086, which indicates that the PP emulator performs slightly better than the low-fidelity simulator. The PP cokriging emulator has NSME 0.998, which indicates that the PP cokriging emulator performs much better than the low-fidelity simulator and the PP emulator.

In our application, the high-fidelity simulator is about 10 times slower than the low-fidelity simulator. Increasing the number of model runs in the high-fidelity simulator is therefore computationally prohibitive. The computational cost of predicting a new high-fidelity model run via the PP cokriging model is negligible compared to that needed to get a single run from the actual SWAN + ADCIRC simulator. This implies that emulating the high-fidelity simulator by using the our proposed PP cokriging model that combines only a small number of high-fidelity runs and a few hundred low-fidelity runs is preferable than using the low-fidelity simulator, in terms of both accuracy and computational cost. The capability to use the low fidelity simulator, without substantial loss of accuracy through use of the PP cokriging model, to explore more of the parameter space greatly enhances the feasibility of achieving high-precision modeling results without a massive computational budget.

Table 2. Predictive performance of emulators at $n^* = 166$ held-out inputs over all N = 9,284 spatial locations. PP= parallel partial.

	RMSPE	CVG(95%)	ALCI(95%)	CRPS	NSME
PP emulator	0.151	0.910	0.512	0.135	-1.086
PP cokriging	0.043	0.993	0.306	0.051	0.998

4.2 Uncertainty Analysis

Cross-validation in the previous section showed that the PP cokriging model can provide very accurate predictions when compared to the true high-fidelity surge model runs in an overall sense. Figure 5 compares the predicted storm surges against held-out storm surge from the high-fidelity surge model across N=9,284 spatial locations at two storm inputs that are used in Figure 2 and Figure 4. At these two inputs, the PP cokriging model seems to have large predictive uncertainties in the southeast region of Cape Coral and to have small predictive uncertainties in the Pine Island Sound Aquatic Preserve and the Caloosahatchee River. The largest predictive standard deviation in the PP cokriging model across all spatial locations is around 0.2, which is smaller than the difference between the high-fidelity surge model and the low-fidelity surge model. This indicates that the PP cokriging model can better approximate the high-fidelity surge model than the low-fidelity surge model at these two inputs in Cape Coral.

Next, we explore the relationship between storm inputs and error structures in the PP cokriging model. We compute the prediction errors across all spatial locations at all held-out inputs. The scatter plot of emulation error against each storm parameter in Figure 6 shows that the majority of emulation errors range from -0.5 to 0.5. This indicates that the PP cokriging model can capture the input-output relationship quite well. As we can see, the emulation errors become larger as the central pressure deficit and the forward speed increase. The scale pressure radius seems to impact the emulation error in an opposite way as central pressure deficit. The emulation errors across different spatial locations are different as shown in Figure 6. This indicates that the current PP cokriging model can capture part

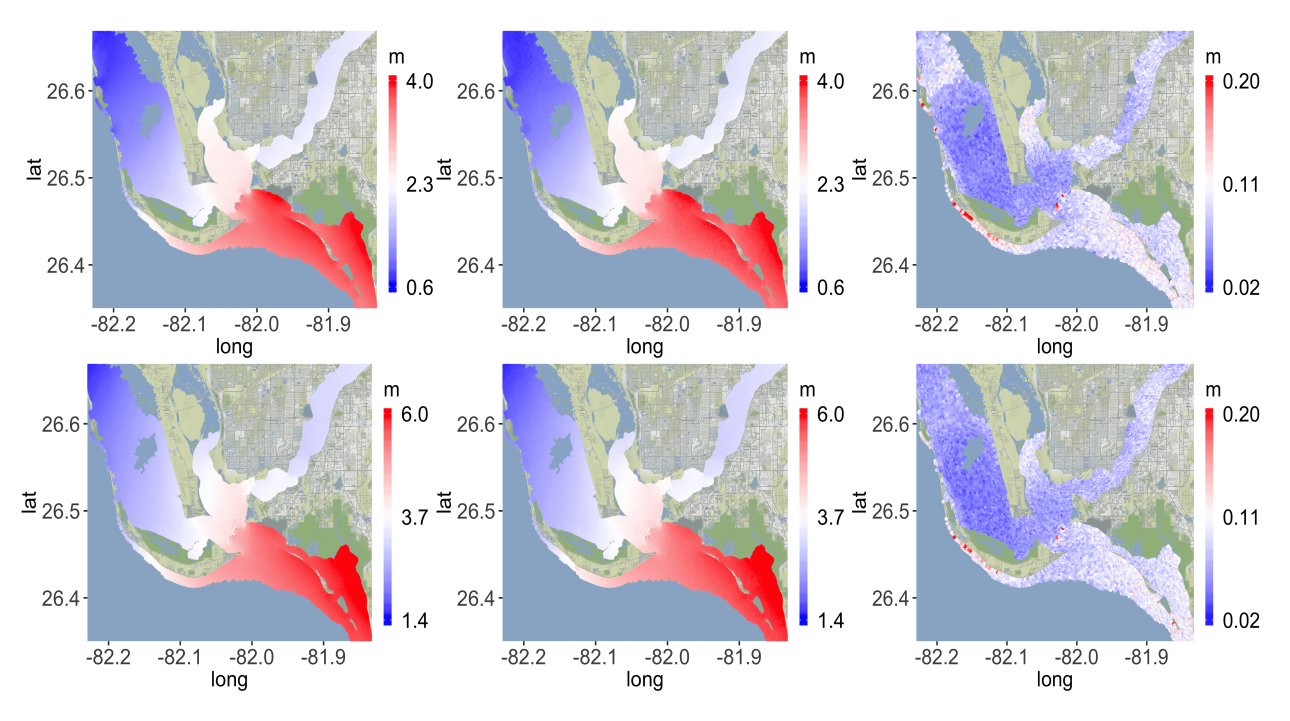


Fig. 5. High-fidelity runs and predicted peak surge elevations with predictive standard errors at two input settings. The first column shows the high-fidelity runs at two different input settings. The second and third columns show the corresponding predicted PSE and associated predictive standard errors.

of the inhomogeneous structures in the output space, and some variations due to inputs are still left. We discuss how we can introduce nonstationarity in input space in Section 5.

Finally, we show the parameter estimates for β_1 , σ_1 , β_2 , γ_1 , and σ_2 in Figure 7. As we can see, these estimated parameters show strong spatially-varying structures at different regions. The estimated regression parameters $\hat{\beta}_1$ and standard deviation $\hat{\sigma}_1$ at the low-fidelity level seem to be smoother than those estimates at fidelity level 2. This is because more variations are captured by the Gaussian process at the low-fidelity level. The remaining variations captured by the discrepancy function $\delta_{2,j}(\cdot)$ are small. This implies that the Gaussian process at the low-fidelity level fits well with model runs from the ADCIRC simulator and the discrepancy between the low-fidelity simulator and the high-fidelity simulator is relatively small. The estimated scale discrepancy parameters $\hat{\gamma}_1$ at all locations also show strongly heterogeneous spatial structures with values slightly greater than 1. This indicates that the high-fidelity simulator is more likely to generate higher values of storm surges than the low-fidelity simulator, but this trend is very small. The estimated standard deviations $\hat{\sigma}_1$ and $\hat{\sigma}_2$ seem to have more local structures than their corresponding regression parameters. This makes sense because we expect the regression trend in Gaussian processes to capture large-scale variations, and covariance structure to capture small-scale variations.

5 Discussion

This article develops a methodology called parallel partial autoregressive cokriging with the capability to emulate a highly complex and computationally demanding high-fidelity storm surge model and provides the necessity for accurate coastal flooding analysis. The parallel cokriging emulator is able to predict highly accurate storm surges in Cape Coral of Southwestern Florida and is as accurate as the high-fidelity SWAN + ADCIRC simulator. The proposed methodology can be also used in a wide range of applications in physical science and engineering when prediction of real-world processes involves multiple computer

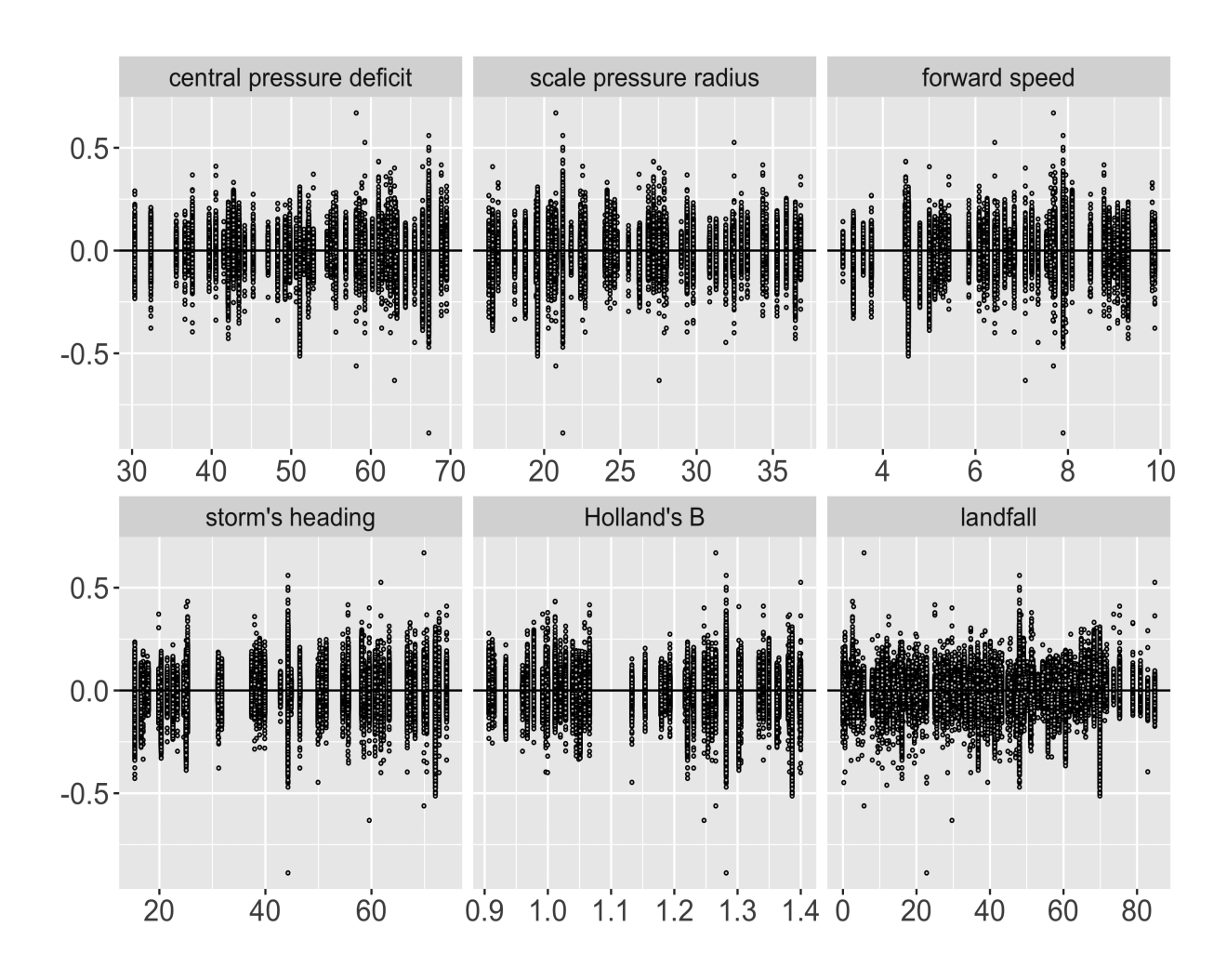


Fig. 6. Prediction errors across all N=9,284 spatial locations against each storm parameter at all held-out inputs.

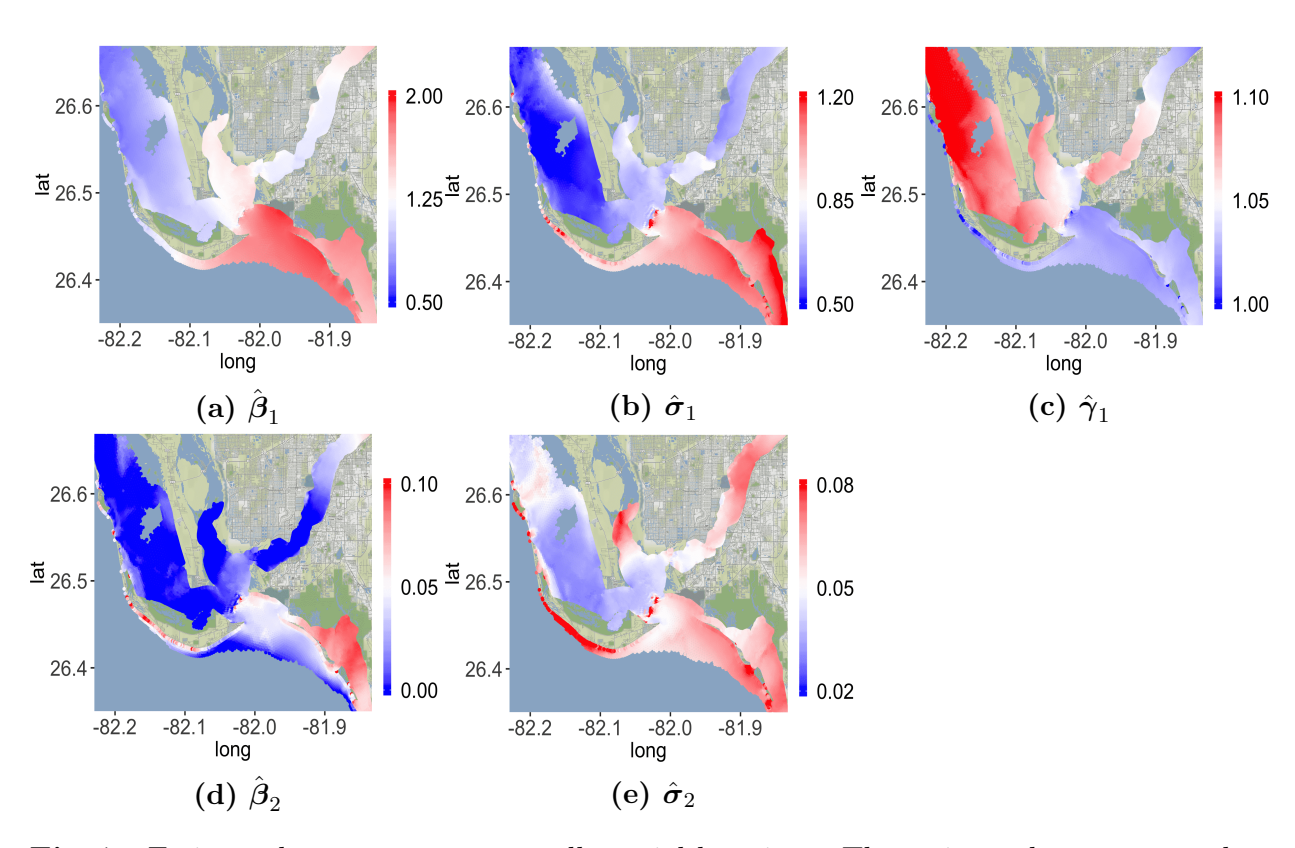


Fig. 7. Estimated parameters across all spatial locations. The estimated parameters show strong heterogeneous spatial patterns.

models with high-dimensional output at different fidelity levels. In real applications, the high-fidelity computer model is more expensive to run than the low-fidelity computer model. The proposed formulation can synthesize output from both low-fidelity and high-fidelity computer models with non-nested designs at each fidelity level. The parallel partial cokriging model has a linear computational cost in terms of output values and also induces nonstationarity in output space, which is crucial to deal with non-smooth surface in output space.

The assumption of independent Gaussian processes at each spatial coordinate seems to be limiting. However, this assumption leads to a separable covariance structure between input space and output space, which has been widely adopted in computer experiments to simplify computations. Due to the independence assumption, emulator predictions at nearby spatial locations can differ a lot and this can help capture rough simulator output. In risk assessment of storm surge hazards, the marginal distribution is needed to compute the rare-event probability. The proposed methodology has the capability to obtain this marginal distribution in a computationally efficient way over a large spatial domain. If interest lies in joint modeling across spatial locations, one can choose a spatial window to enable joint modeling. A related concern is the assumption of common correlation parameters at all spatial locations. If correlation parameters differ at each spatial location, the computational cost would not be linear in terms of model output. This is a key advantage when the hazard from storm surge is assessed over a large spatial domain. One can potentially partition the domain into a set of subregions and allow different correlation parameters across these subregions.

Several extensions of the proposed approach can be pursued in future work. Many applications in computer experiments have small number of computer model runs, however, when the real application is extremely complex, large number of model runs are required to explore the input space so that the emulator can be trained more accurately. This problem can be tackled either via computationally efficient Gaussian process approximation approaches (e.g. Gramacy and Apley, 2015) or via sequential design (Le Gratiet and Cannamela, 2015).

The former handles the computational issue directly via fast approximations, and the latter selects model runs sequentially to improve the emulator's performance. Another extension is to deal with nonstationarity in input space for complex real applications. For instance, one can introduce nonstationarity via treed Gaussian process (Gramacy and Lee, 2008; Konomi and Karagiannis, 2019).

Finally, the parallel partial cokriging methodology provides an efficient way to generate high-fidelity storm surges over a large domain in space or storm parameter space. These are applicable across a wide range of storm surge work. Most notably, this method should enable more precise, lower-cost estimation of flood hazards across a wide range of event probabilities. These analyses support hazard delineation for insurance rate maps, siting of critical infrastructure, design and planning of coastal protections.

Acknowledgements

This material is partly supported by the U.S. NSF under Grant DMS-1638521 to the Statistical and Applied Mathematical Sciences Institute, by the U.S. NSF under Grant Award Number ACI-1339723, and by the U.S. Department of Homeland Security under Grant Award Number 2015-ST-061-ND0001-01. The views and conclusions contained in this document are those of the authors and should not be interpreted as necessarily representing the official policies, either expressed or implied, of the U.S. NSF and the U.S Department of Homeland Security. This work used the Extreme Science and Engineering Discovery Environment (XSEDE) Lonestar5 and Stampede2 at the Texas Advanced Computing Center (TACC) through allocation DMS180042. The first author (Pulong Ma) would like to thank Professor James O. Berger for his valuable guidance.

Appendix

A Useful Results

Lemma 1 (One-Step Prediction). The mean $m_{s,j}(\mathbf{x}_0)$ and variance $v_{s,j}(\mathbf{x}_0)$ in the conditional predictive distribution $\pi(y_{s,j}(\mathbf{x}_0) \mid \tilde{\mathbf{y}}_j^{\mathscr{D}}, \boldsymbol{\beta}_j, \boldsymbol{\gamma}_j, \boldsymbol{\sigma}_j^2, \boldsymbol{\phi})$ are given by

$$m_{s,j}(\mathbf{x}_0) = \mathbf{f}_j^{\top}(\mathbf{x}_0)\boldsymbol{\beta}_j + \mathbf{c}_j^{\top}(\mathbf{x}_0)\boldsymbol{\Sigma}^{j,-1}(\mathbf{y}_j^{\mathscr{D}} - \tilde{\mathbf{F}}^j\boldsymbol{\beta}_j),$$

$$v_{s,j}(\mathbf{x}_0) = \sigma_{s,j}^2 r(\mathbf{x}_0, \mathbf{x}_0 | \boldsymbol{\phi}_s) - \mathbf{c}_j^{\top}(\mathbf{x}_0)\boldsymbol{\Sigma}^{j,-1}\mathbf{c}_j(\mathbf{x}_0),$$
(A.1)

where the vector $\mathbf{f}_i(\mathbf{x}_0)$ is given by

$$\mathbf{f}_j(\mathbf{x}_0) := \left(\left(\prod_{i=1}^{s-1} \gamma_{i,j} \right) \tilde{\mathbf{h}}_1^\top(\mathbf{x}_0), \left(\prod_{i=2}^{s-1} \gamma_{i,j} \right) \tilde{\mathbf{h}}_2^\top(\mathbf{x}_0), \ldots, \gamma_{s-1,j} \tilde{\mathbf{h}}_{s-1}^\top(\mathbf{x}_0), \tilde{\mathbf{h}}_s^\top(\mathbf{x}_0) \right)^\top.$$

 Σ^{j} is an s-by-s block matrix with the (i,i')-th block of size \tilde{n}_{t} -by- \tilde{n}_{t} given by

$$\Sigma_{i,i}^{j}(\tilde{\mathcal{X}}_{t},\tilde{\mathcal{X}}_{t}) := \begin{cases} \sum_{k=1}^{t} \left(\prod_{\ell=k}^{t-1} \gamma_{\ell,j}^{2} \right) \sigma_{k,j}^{2} r(\tilde{\mathcal{X}}_{t},\tilde{\mathcal{X}}_{t} \mid \boldsymbol{\phi}_{k}), & \text{for } i = i'; \\ \left(\prod_{k=i}^{i'-1} \gamma_{k,j} \right) \Sigma_{i,i}^{j}(\tilde{\mathcal{X}}_{i},\tilde{\mathcal{X}}_{i}'), & \text{for } i < i'. \end{cases}$$

The vector $\mathbf{c}_j(\mathbf{x}_0)$ is $\mathbf{c}_j(\mathbf{x}_0) := (\mathbf{c}_{1,j}(\mathbf{x}_0, \tilde{\mathcal{X}}_1), \dots, \mathbf{c}_{s,j}(\mathbf{x}_0, \tilde{\mathcal{X}}_s))^{\top}$ with

$$\mathbf{c}_{t,j}(\mathbf{x}_0, \tilde{\mathcal{X}}_t) = \gamma_{t-1,j} \mathbf{c}_{t-1,j}(\mathbf{x}_0, \tilde{\mathcal{X}}_t) + \left(\prod_{k=t}^{s-1} \gamma_{k,j}\right) \sigma_{t,j}^2 r(\mathbf{x}_0, \tilde{\mathcal{X}}_t | \boldsymbol{\phi}_t), \qquad t = 2, \dots, s,$$

where $\prod_{k=s}^{s-1} \gamma_{k,j} := 1$ for all j's and $\mathbf{c}_{1,j}(\mathbf{x}_0, \tilde{\mathcal{X}}_1) := \left(\prod_{k=t}^{s-1} \gamma_{k,j}\right) \sigma_{1,j}^2 r(\mathbf{x}_0, \tilde{\mathcal{X}}_1 | \boldsymbol{\phi}_1)$. The (i, k)th block in the matrix $\tilde{\mathbf{F}}^j$ is $\tilde{\mathbf{F}}^j_{i,k} := \prod_{t=k}^{i-1} \gamma_{t,j} \mathbf{h}_k(\tilde{\mathcal{X}}_i)$ for $i \geq k$, and $\tilde{\mathbf{F}}^j_{i,k} := \mathbf{0}$ for i < k.

Proof. In the univariate setting, this formula is the same as the one in Kennedy and O'Hagan (2000); Le Gratiet (2013); Qian and Wu (2008). As the predictive distribution is independent given the range parameters, the result follows straightforwardly for spatial coordinate j. \square

Lemma 2. Let
$$\mathbf{T}_{t,j} := [\mathbf{H}_t, W_{t-1,j}]$$
 and $\mathbf{Q}_t := \mathbf{R}_t^{-1} \{ \mathbf{I} - \mathbf{T}_{t,j} (\mathbf{T}_{t,j}^\top \mathbf{R}_t^{-1} \mathbf{T}_{t,j})^{-1} \mathbf{T}_{t,j}^\top \mathbf{R}_t^{-1} \}$ for

t > 1. Then the following result holds:

 $S^{2}(\boldsymbol{\phi}_{t},\mathbf{y}_{t,j}) = \mathbf{y}_{t,j}^{\top} \mathbf{Q}_{t}^{H} \mathbf{y}_{t,j} - \mathbf{y}_{t,j}^{\top} \mathbf{K}_{t} \boldsymbol{\Omega}_{t-1,j} \mathbf{K}_{t} \mathbf{y}_{t,j} + 2 \mathbf{y}_{t,j}^{\top} \mathbf{R}_{t}^{-1} \boldsymbol{\Omega}_{t-1,j} \mathbf{K}_{t} \mathbf{y}_{t,j} - \mathbf{y}_{t,j}^{\top} \mathbf{R}_{t}^{-1} \boldsymbol{\Omega}_{t-1,j} \mathbf{R}_{t}^{-1} \mathbf{y}_{t,j}$ $where \ \mathbf{Q}_{t}^{H} := \mathbf{R}_{t}^{-1} \{ \mathbf{I} - \mathbf{H}_{t} (\mathbf{H}_{t}^{\top} \mathbf{R}_{t}^{-1} \mathbf{H}_{t})^{-1} \mathbf{H}_{t}^{\top} \mathbf{R}_{t}^{-1} \}, \ \mathbf{K}_{t} := \mathbf{R}_{t}^{-1} \mathbf{H}_{t} (\mathbf{H}_{t}^{\top} \mathbf{R}_{t}^{-1} \mathbf{H}_{t})^{-1} \mathbf{H}_{t}^{\top} \mathbf{R}_{t}^{-1}, \ and$ $\boldsymbol{\Omega}_{t-1,j} := W_{t-1,j} (W_{t-1,j}^{\top} \mathbf{Q}_{t}^{H} W_{t-1,j})^{-1} W_{t-1,j}^{\top}. \ These \ two \ identities \ show \ that \ the \ computational$ $cost \ to \ compute \ \sum_{j=1}^{N} \ln |\mathbf{T}_{t,j}^{\top} \mathbf{R}_{t}^{-1} \mathbf{T}_{t,j}| \ and \ \sum_{j=1}^{N} \ln S^{2}(\boldsymbol{\phi}_{t}, \mathbf{y}_{t,j}) \ is \ reduced \ from \ O(Nn_{t}^{3}) \ to$ $O(n_{t}^{3} + Nn_{t}^{2})$

Proof of Lemma 2. Notice that

$$\mathbf{T}_{t,j}^{\top}\mathbf{R}_{t}^{-1}\mathbf{T}_{t,j} = \begin{pmatrix} \mathbf{H}_{t}^{\top}\mathbf{R}_{t}^{-1}\mathbf{H}_{t} & \mathbf{H}_{t}^{\top}\mathbf{R}_{t}^{-1}W_{t-1,j} \\ W_{t-1,j}^{\top}\mathbf{R}_{t}^{-1}\mathbf{H}_{t} & W_{t-1,j}^{\top}\mathbf{R}_{t}^{-1}W_{t-1,j} \end{pmatrix},$$

$$(\mathbf{T}_{t,j}^{\top}\mathbf{R}_{t}^{-1}\mathbf{T}_{t,j})^{-1} = \begin{pmatrix} \mathbf{A}_{t}^{-1} + \mathbf{A}_{t}^{-1}\mathbf{H}_{t}^{\top}\mathbf{R}_{t}^{-1}\Omega_{t-1,j}\mathbf{R}_{t}^{-1}\mathbf{H}_{t}\mathbf{A}_{t}^{-1} & -\mathbf{A}_{t}^{-1}\mathbf{H}_{t}^{\top}\mathbf{R}_{t}^{-1}W_{t-1,j}\omega_{t-1} \\ -\omega_{t-1}W_{t-1,j}^{\top}\mathbf{R}_{t}^{-1}\mathbf{H}_{t}\mathbf{A}_{t}^{-1} & \omega_{t-1} \end{pmatrix},$$

where $\omega_{t-1} := (W_{t-1,j}^{\top} \mathbf{Q}_t^H W_{t-1,j})^{-1}$ and $\mathbf{A}_t = \mathbf{H}_t^{\top} \mathbf{R}_t^{-1} \mathbf{H}_t$. Using block matrix determinant yield the formula to compute the determinant of $\mathbf{T}_{t,j}^{\top} \mathbf{R}_t^{-1} \mathbf{T}_{t,j}$. Using the block matrix inverse yields

$$\begin{split} \mathbf{T}_{t,j}(\mathbf{T}_{t,j}^{\top}\mathbf{R}_{t}^{-1}\mathbf{T}_{t,j})^{-1}\mathbf{T}_{t,j}^{\top} &= \mathbf{H}_{t}\mathbf{A}_{t}^{-1}\mathbf{H}_{t}^{\top} + \mathbf{H}_{t}\mathbf{A}_{t}^{-1}\mathbf{H}_{t}^{\top}\mathbf{R}_{t}^{-1}\boldsymbol{\Omega}_{t-1,j}\mathbf{R}_{t}^{-1}\mathbf{H}_{t}\mathbf{A}_{t}^{-1}\mathbf{H}_{t}^{\top} \\ &- W_{t-1,j}\omega_{t-1}W_{t-1,j}^{\top}\mathbf{R}_{t}^{-1}\mathbf{H}_{t}\mathbf{A}_{t}^{-1}\mathbf{H}_{t}^{\top} \\ &- \mathbf{H}_{t}\mathbf{A}_{t}^{-1}\mathbf{H}_{t}^{\top}\mathbf{R}_{t}^{-1}W_{t-1,j}\omega_{t-1}W_{t-1,j}^{\top} + W_{t-1,j}\omega_{t-1}W_{t-1,j}^{\top}. \end{split}$$

Standard calculation will yield the formula to compute $S^2(\phi_t, \mathbf{y}_{t,j})$.

B Distributions

It is straightforward to show that the conditional distribution $\pi(\mathring{\mathbf{y}}_j^{\mathscr{D}} \mid \mathbf{y}_j^{\mathscr{D}}, \boldsymbol{\beta}_j, \boldsymbol{\gamma}_j, \boldsymbol{\sigma}_j^2, \boldsymbol{\phi})$ can be factorized as

$$\pi(\mathring{\mathbf{y}}_{j}^{\mathscr{D}} \mid \mathbf{y}_{j}^{\mathscr{D}}, \boldsymbol{\beta}_{j}, \boldsymbol{\gamma}_{j}, \boldsymbol{\sigma}_{j}^{2}, \boldsymbol{\phi}) = \pi(\mathring{\mathbf{y}}_{1}^{\mathscr{D}} \mid \mathbf{y}_{1}^{\mathscr{D}}, \boldsymbol{\beta}_{1,j}, \sigma_{1,j}^{2}, \boldsymbol{\phi}_{1}) \prod_{t=2}^{s-1} \pi(\mathring{\mathbf{y}}_{t}^{\mathscr{D}} \mid \mathring{\mathbf{y}}_{t-1}^{\mathscr{D}}, \mathbf{y}_{t}^{\mathscr{D}}, \boldsymbol{\beta}_{t,j}, \gamma_{t-1,j}, \sigma_{t,j}^{2}, \boldsymbol{\phi}_{t}).$$

The conditional distributions are multivariate normal distributions with means and variances given by

$$\mu_{\mathring{y}|y}^{t,j} := \mathring{\mathbf{T}}_{t,j} \mathbf{b}_{t,j} + r(\mathring{\mathcal{X}}_t, \mathcal{X}_t \mid \boldsymbol{\phi}_t) \mathbf{R}_t^{-1} (\mathbf{y}_{t,j} - \mathbf{T}_{t,j} \mathbf{b}_{t,j}),$$

$$\Sigma_{\mathring{y}|y}^{t,j} := \sigma_{t,j}^2 \{ r(\mathring{\mathcal{X}}_t, \mathring{\mathcal{X}}_t \mid \boldsymbol{\phi}_t) - r(\mathring{\mathcal{X}}_t, \mathcal{X}_t \mid \boldsymbol{\phi}_t) \mathbf{R}_t^{-1} r(\mathcal{X}_t, \mathring{\mathcal{X}}_t \mid \boldsymbol{\phi}_t) \},$$

where $\mathring{\mathbf{T}}_{1,j} := \mathring{\mathbf{H}}_{1,j}, \ \mathring{\mathbf{T}}_{t,j} := [\mathring{\mathbf{H}}_{1,j}, y_{t-1,j}(\mathring{\mathcal{X}}_t)] \text{ for } t > 1, \ \mathbf{b}_{1,j} = \boldsymbol{\beta}_1, \text{ and } \mathbf{b}_{t,j} = (\boldsymbol{\beta}_{t,j}^\top, \gamma_{t-1,j})^\top$ with $t = 2, \dots, s$.

The joint distribution of $\tilde{\mathbf{y}}^{\mathscr{D}}$ and $\boldsymbol{\phi}$ can be obtained via $\pi(\tilde{\mathbf{y}}^{\mathscr{D}}, \boldsymbol{\phi}) = \pi(\tilde{\mathbf{y}}^{\mathscr{D}} \mid \boldsymbol{\phi})\pi(\boldsymbol{\phi})$. Suppose that the missing data $\mathring{\mathbf{y}}_t$ only depends on \mathbf{y}_t and missing data $\mathring{\mathbf{y}}_{t-1}$. It follows that, the conditional distribution $\pi(\mathring{\mathbf{y}}^{\mathscr{D}} \mid \mathbf{y}^{\mathscr{D}}, \boldsymbol{\phi})$ is given by

$$\pi(\mathring{\mathbf{y}}^{\mathscr{D}} \mid \mathbf{y}^{\mathscr{D}}, \boldsymbol{\phi}) = \prod_{j=1}^{N} \pi(\mathring{\mathbf{y}}_{1,j} \mid \mathbf{y}_{1,j}, \boldsymbol{\phi}_{1}) \prod_{t=2}^{s-1} \pi(\mathring{\mathbf{y}}_{t,j} \mid \tilde{\mathbf{y}}_{t-1,j}, \mathbf{y}_{t,j}, \boldsymbol{\phi}_{t}),$$

where the conditional distributions on the right-hand side are \mathring{n}_t -dimensional Student-t distribution for t = 1, ..., s - 1, whose degrees of freedom is $n_t - q_t$, location parameters $\mu_{t,j}$ and scale parameters $V_{t,j}$ are

$$\boldsymbol{\mu}_{t,j} := \mathring{\mathbf{T}}_t \hat{\mathbf{b}}_{t,j} + r(\mathring{\mathcal{X}}_t, \mathcal{X}_t \mid \boldsymbol{\phi}_t) \mathbf{R}_t^{-1} (\mathbf{y}_{t,j} - \mathbf{T}_{t,j} \hat{\mathbf{b}}_{t,j}),$$

$$V_{t,j} := \frac{S^2(\boldsymbol{\phi}_t, \mathbf{y}_{t,j})}{n_t - q_t} \Sigma_{\mathring{y}\mathring{y}|y}^t,$$

with

$$\begin{split} \hat{\mathbf{b}}_{t,j} &:= (\mathbf{T}_{t,j}^{\top} \mathbf{R}_t^{-1} \mathbf{T}_{t,j})^{-1} \mathbf{T}_{t,j}^{\top} \mathbf{R}_t^{-1} \mathbf{y}_{t,j} \\ S^2(\boldsymbol{\phi}_t, \mathbf{y}_{t,j}) &:= \mathbf{y}_{t,j}^{\top} \mathbf{Q}_t \mathbf{y}_{t,j} \\ \Sigma_{\mathring{y}\mathring{y}|y}^t &:= \mathring{\mathbf{R}}_t - \mathbf{r}_t^{\top} (\mathring{\mathcal{X}}_t) \mathbf{R}_t^{-1} \mathbf{r}_t (\mathring{\mathcal{X}}_t) + [\mathring{\mathbf{T}}_{t,j}^{\top} - \mathbf{T}_{t,j}^{\top} \mathbf{R}_t^{-1} \mathbf{r}_t (\mathring{\mathcal{X}}_t)]^{\top} (\mathbf{T}_{t,j}^{\top} \mathbf{R}_t^{-1} \mathbf{T}_{t,j})^{-1} \\ &\cdot [\mathring{\mathbf{T}}_{t,j}^{\top} - \mathbf{T}_{t,j}^{\top} \mathbf{R}_t^{-1} \mathbf{r}_t (\mathring{\mathcal{X}}_t)], \end{split}$$

where $\mathbf{R}_t := r(\mathcal{X}_t, \mathcal{X}_t \mid \boldsymbol{\phi}_t), \ \mathbf{r}_t(\mathring{\mathcal{X}}_t) := r(\mathcal{X}_t, \mathring{\mathcal{X}}_t \mid \boldsymbol{\phi}_t), \ \text{and} \ \mathring{\mathbf{R}}_t := r(\mathring{\mathcal{X}}_t, \mathring{\mathcal{X}}_t \mid \boldsymbol{\phi}_t). \ \mathbf{Q}_t := \mathbf{R}_t^{-1}\{\mathbf{I} - \mathbf{T}_{t,j}(\mathbf{T}_{t,j}^{\top}\mathbf{R}_t^{-1}\mathbf{T}_{t,j})^{-1}\mathbf{T}_{t,j}^{\top}\mathbf{R}_t^{-1}\}.$

References

- Aerts, J. C., Botzen, W. W., Emanuel, K., Lin, N., De Moel, H., and Michel-Kerjan, E. O. (2014). Evaluating flood resilience strategies for coastal megacities. *Science*, 344(6183):473–475.
- Aerts, J. C., Lin, N., Botzen, W., Emanuel, K., and de Moel, H. (2013). Low-probability flood risk modeling for New York City. *Risk Analysis*, 33(5):772–788.
- Bilskie, M. V., Hagen, S., and Irish, J. (2019). Development of return period stillwater floodplains for the northern Gulf of Mexico under the coastal dynamics of sea level rise. *Journal of Waterway, Port, Coastal, and Ocean Engineering*, 145(2):04019001.
- Blanton, B., Dresback, K., Colle, B., Kolar, R., Vergara, H., Hong, Y., Leonardo, N., Davidson, R., Nozick, L., and Wachtendorf, T. (2018). An integrated scenario ensemble-based framework for hurricane evacuation modeling: Part 2—hazard modeling. *Risk analysis*.
- Booij, N., Ris, R. C., and Holthuijsen, L. H. (1999). A third-generation wave model for coastal regions: 1. Model description and validation. *Journal of Geophysical Research:* Oceans, 104(C4):7649–7666.
- Bunya, S., Dietrich, J. C., Westerink, J. J., Ebersole, B. A., Smith, J. M., Atkinson, J. H., Jensen, R., Resio, D. T., Luettich, R. A., Dawson, C., Cardone, V. J., Cox, A. T., Powell, M. D., Westerink, H. J., and Roberts, H. J. (2010). A high-resolution coupled riverine flow, tide, wind, wind wave, and storm surge model for southern Louisiana and Mississippi. Part I: Model development and validation. *Monthly Weather Review*, 138(2):345–377.
- Cardone, V. J. and Cox, A. T. (2009). Tropical cyclone wind field forcing for surge models: critical issues and sensitivities. *Natural Hazards*, 51(1):29–47.
- Cialone, M. A., Grzegorzewski, A. S., Mark, D. J., Bryant, M. A., and Massey, T. C. (2017). Coastal-storm model development and water-level validation for the North Atlantic

- coast comprehensive study. Journal of Waterway, Port, Coastal, and Ocean Engineering, 143(5):04017031.
- Conti, S. and O'Hagan, A. (2010). Bayesian emulation of complex multi-output and dynamic computer models. *Journal of Statistical Planning and Inference*, 140(3):640–651.
- Cressie, N. (1993). Statistics for Spatial Data. John Wiley & Sons, New York, revised edition.
- de Moel, H. and Aerts, J. (2011). Effect of uncertainty in land use, damage models and inundation depth on flood damage estimates. *Natural Hazards*, 58(1):407–425.
- Dietrich, J., Bunya, S., Westerink, J., Ebersole, B., Smith, J., Atkinson, J., Jensen, R., Resio, D., Luettich, R., Dawson, C., et al. (2010). A high-resolution coupled riverine flow, tide, wind, wind wave, and storm surge model for southern Louisiana and Mississippi. Part II: Synoptic description and analysis of hurricanes Katrina and Rita. Monthly Weather Review, 138(2):378–404.
- Dietrich, J., Zijlema, M., Westerink, J., Holthuijsen, L., Dawson, C., Luettich, R., Jensen, R., Smith, J., Stelling, G., and Stone, G. (2011). Modeling hurricane waves and storm surge using integrally-coupled, scalable computations. *Coastal Engineering*, 58(1):45 65.
- Dietrich, J. C., Tanaka, S., Westerink, J. J., Dawson, C. N., Luettich, R. A., Zijlema, M., Holthuijsen, L. H., Smith, J. M., Westerink, L. G., and Westerink, H. J. (2012). Performance of the unstructured-mesh, SWAN+ADCIRC model in computing hurricane waves and surge. *Journal of Scientific Computing*, 52(2):468–497.
- FEMA (2006). Hurricane Katrina in the Gulf Coast. Washington, D.C.: Federal Emergency Management Agency.
- FEMA (2008). Mississippi coastal analysis project. Project reports prepared by URS Group Inc., (Graithersburg MD and Tallahassee FL) under HMTAP Contract HSFEHQ-06-D-0162, Task Order 06-J-0018.
- FEMA (2017). Southwest Florida Storm Surge Study Intermediate Data Submittal 2. Report Prepared by the Risk Assessment, Mapping, and Planning Partners (RAMPP) under FEMA IDIQ Contract HSFEHQ-09-D-0369 and Task Order HSFE04-13-J-0097. FEMA Region IV.
- Fischbach, J., Johnson, D., and Kuhn, K. (2016). Bias and efficiency tradeoffs in the selection of storm suites used to estimate flood risk. *Journal of Marine Science and Engineering*, 4(1):10.
- Garner, A. J., Mann, M. E., Emanuel, K. A., Kopp, R. E., Lin, N., Alley, R. B., Horton, B. P., DeConto, R. M., Donnelly, J. P., and Pollard, D. (2017). Impact of climate change on New York City's coastal flood hazard: Increasing flood heights from the preindustrial to 2300 CE. *Proceedings of the National Academy of Sciences*, 114(45):11861–11866.
- Georgas, N., Blumberg, A., Herrington, T., Wakeman, T., Saleh, F., Runnels, D., Jordi Ballester, A., Ying, K., Yin, L., Ramaswamy, V., Yakubovskiy, A., Lopez, O., Mcnally, J., Schulte, J., and Wang, Y. (2016). The stevens flood advisory system: Operational H3E

- flood forecasts for the greater New York/New Jersey metropolitan region. *International Journal of Safety and Security Engineering*, 6(3):648–662.
- Gneiting, T. and Raftery, A. E. (2007). Strictly proper scoring rules, prediction, and estimation. *Journal of the American Statistical Association*, 102(477):359–378.
- Gramacy, R. B. and Apley, D. W. (2015). Local Gaussian process approximation for large computer experiments. *Journal of Computational and Graphical Statistics*, 24(2):561–578.
- Gramacy, R. B. and Lee, H. K. H. (2008). Bayesian treed Gaussian process models with an application to computer modeling. *Journal of the American Statistical Association*, 103(483):1119–1130.
- Gu, M. (2019). Jointly robust prior for Gaussian stochastic process in emulation, calibration and variable selection. *Bayesian Analysis*, 14(3):877–905.
- Gu, M. and Berger, J. O. (2016). Parallel partial Gaussian process emulation for computer models with massive output. *The Annals of Applied Statistics*, 10(3):1317–1347.
- Gu, M., Palomo, J., and Berger, J. O. (2018). RobustGaSP: Robust Gaussian stochastic process emulation in R. arXiv preprint arXiv:1801.01874.
- Hesser, T. J., Cialone, M. A., and Anderson, M. E. (2013). Lake St. Clair: Storm wave and water level modeling.
- Jensen, R. E., Cialone, M. A., Chapman, R. S., Ebersole, B. A., Anderson, M., and Thomas, L. (2012). Lake Michigan storm: Wave and water level modeling.
- Kennedy, M. and O'Hagan, A. (2000). Predicting the output from a complex computer code when fast approximations are available. *Biometrika*, 87(1):1–13.
- Klotzbach, P. J., Bowen, S. G., Pielke Jr, R., and Bell, M. (2018). Continental US hurricane landfall frequency and associated damage: Observations and future risks. *Bulletin of the American Meteorological Society*, 99(7):1359–1376.
- Konomi, B. A. and Karagiannis, G. (2019). Bayesian analysis of multifidelity computer models with local features and non-nested experimental designs: Application to the WRF model. Submitted.
- Le Gratiet, L. (2013). Bayesian analysis of hierarchical multifidelity codes. SIAM/ASA Journal on Uncertainty Quantification, 1(1):244–269.
- Le Gratiet, L. and Cannamela, C. (2015). Cokriging-based sequential design strategies using fast cross-validation techniques for multi-fidelity computer codes. *Technometrics*, 57(3):418–427.
- Liu, Y., Asher, T. G., and Irish, J. L. (2019). Physical drivers of changes in probabilistic surge hazard under sea level rise. *Earth's Future*, 7(7):819–832.
- Longuet-Higgins, M. S. and Stewart, R. (1964). Radiation stresses in water waves; a physical discussion, with applications. In *Deep Sea Research and Oceanographic Abstracts*, volume 11, pages 529–562. Elsevier.

- Luettich, R. and Westerink, J. (2004). Formulation and numerical implementation of the 2D/3D ADCIRC finite element model version 44. xx.
- Ma, P. (2019). Objective Bayesian analysis of a cokriging model for hierarchical multifidelity codes. Under review.
- Marsooli, R. and Lin, N. (2018). Numerical modeling of historical storm tides and waves and their interactions along the US east and Gulf coasts. *Journal of Geophysical Research:* Oceans, 123(5):3844–3874.
- Niedoroda, A., Resio, D., Toro, G., Divoky, D., Das, H., and Reed, C. (2010). Analysis of the coastal Mississippi storm surge hazard. *Ocean Engineering*, 37(1):82–90.
- NOAA National Centers for Environmental Information (2019). U.S. billion-dollar weather and climate disasters. URL: https://www.ncdc.noaa.gov/billions/.
- Pielke Jr, R. A., Gratz, J., Landsea, C. W., Collins, D., Saunders, M. A., and Musulin, R. (2008). Normalized hurricane damage in the United States: 1900–2005. *Natural Hazards Review*, 9(1):29–42.
- Qian, P. Z. G. and Wu, C. F. J. (2008). Bayesian hierarchical modeling for integrating low-accuracy and high-accuracy experiments. *Technometrics*, 50(2):192–204.
- Rappaport, E. N. (2014). Fatalities in the United States from Atlantic tropical cyclones: New data and interpretation. *Bulletin of the American Meteorological Society*, 95(3):341–346.
- Sacks, J., Welch, W. J., Mitchell, T. J., and Wynn, H. P. (1989). Design and analysis of computer experiments. *Statistical Science*, 4(4):409–435.
- Stein, M. L. (1999). Interpolation of Spatial Data: Some Theory for Kriging. Springer Science & Business Media.
- Tanaka, S., Bunya, S., Westerink, J. J., Dawson, C., and Luettich, R. A. (2011). Scalability of an unstructured grid continuous Galerkin based hurricane storm surge model. *Journal of Scientific Computing*, 46(3):329–358.
- Toro, G., Niedoroda, A., Reed, C., and Divoky, D. (2010). Quadrature-based approach for the efficient evaluation of surge hazard. *Ocean Engineering*, 37(1):114 124. A Forensic Analysis of Hurricane Katrina's Impact: Methods and Findings.
- Towns, J., Cockerill, T., Dahan, M., Foster, I., Gaither, K., Grimshaw, A., Hazlewood, V., Lathrop, S., Lifka, D., Peterson, G. D., Roskies, R., Scott, J. R., and Wilkins-Diehr, N. (2014). XSEDE: Accelerating scientific discovery. *Computing in Science & Engineering*, 16(5):62–74.
- Wamsley, T., Godsey, E., Bunch, B. W., Chapman, R. S., Gravens, M. B., Grzegorzewski, A. S., Johnson, B. D., King, D. B., Permenter, R. L., and Tillman, D. L. (2013). Mississippi coastal improvement program, barrier island restoration numerical modeling.
- Wei, G. C. G. and Tanner, M. A. (1990). A Monte Carlo implementation of the EM algorithm and the poor man's data augmentation algorithms. *Journal of the American Statistical Association*, 85(411):699–704.

- Westerink, J. J., Luettich, R. A., Feyen, J. C., Atkinson, J. H., Dawson, C., Roberts, H. J., Powell, M. D., Dunion, J. P., Kubatko, E. J., and Pourtaheri, H. (2008). A basin-to channel-scale unstructured grid hurricane storm surge model applied to southern Louisiana. *Monthly weather review*, 136(3):833–864.
- Yin, J., Lin, N., and Yu, D. (2016). Coupled modeling of storm surge and coastal inundation: A case study in New York City during Hurricane Sandy. *Water Resources Research*, 52(11):8685–8699.
- Zijlema, M. (2010). Computation of wind-wave spectra in coastal waters with SWAN on unstructured grids. *Coastal Engineering*, 57(3):267 277.